SLAC – PUB – 3213 (REV.)
June 1986
(A)

Surface Properties of Metal-Nitride and Metal-Carbide Films Deposited on Nb for Radio-Frequency Superconductivity*

E.L. GARWIN, F.K. KING, R.E. KIRBY

Stanford Linear Accelerator Center
Stanford University, Stanford, California, 94305

and

O. AITA

College of Engineering, University of Osaka Prefecture,
Mozu, Sakai, Osaka 591, Japan

Submitted to *Journal of Applied Physics*

* Work supported by the Department of Energy, contract DE – AC03 – 76SF00515.

ABSTRACT

Various effects occur which can prevent attainment of the high Q's and/or the high gradient fields necessary for the operation of rf superconducting cavities. One of these effects, multipactor, both causes the cavity to detune during filling due to resonant secondary electron emission at the cavity walls, and lowers the Q by dissipative processes. TiN deposited onto the high field regions of room temperature Al cavities has been used at SLAC to successfully reduce multipactor in the past. We have therefore studied TiN and its companion materials, NbN, NbC, and TiC, all on Nb substrates under several realistic conditions: 1) as deposited, 2) exposed to air, and 3) electron-bombarded. The studied films (up to 14 nm thickness) were sputter deposited onto sputter-cleaned Nb substrates. Results indicate that all the materials tested gave substantially the same results. The maximum secondary electron yields for as-deposited films were reduced to nearly the pre-oxidized values after electron bombardment (2-3 x 10^{17} electrons-cm^{-2} in the case of NbN and NbC). XPS analysis showed that the oxides (e.g. TiO_2 in the case of TiN films) formed during air exposure were slightly reduced (converted to lower oxides) by the electron beam exposure. AES showed a slight reduction in the surface O concentration following beam exposure. These results suggest that the chemical nature of top surface layers is responsible for the substantial changes in secondary electron yield observed upon electron beam exposures and that AES does not reflect this change strongly because of the difficulty in extracting chemical (versus elemental)information from AES. The results indicate that any of these films would be poor choices if simply deposited and exposed to air, but, in fact, the in-situ electron bombardment which occurs during cavity operation serves to reduce the secondary electron yield and thereby causes a substantial reduction in multipacting.

1. Introduction

Electron loading in rf superconducting cavity structures constitutes a major problem in the application of superconducting technology to storage rings and accelerators. In recent years new choices of cavity geometries which inhibit multipacting have been successfully applied to the construction of superconducting accelerator structures. The problem remains, however, of decreasing or eliminating the effects of multipacting in parts of the structures for which the geometry cannot be significantly changed, such as in higher-order-mode couplers. In these cases the suppression of multipacting can be achieved by coating the surfaces of interest with a material which must have both a low secondary electron emission (SEE) coefficient and low rf losses, in order to maintain the original high unloaded Q of the cavity. Materials such as NbC, NbN, TiC and TiN seem to be good candidates for this purpose(1). They are good electrical conductors and possess rather high superconducting transition temperatures(2).

TiN is routinely used at SLAC as a proven anti-multipactor coating for intercavity coupling slots, rf windows and rf coupling loops on normal conductor surfaces. Preliminary surface physics studies on this material indicated that as-deposited films exhibited low SEE yields, but exposure to air caused the SEE yields to increase so much that such films would appear useless as anti-multipactor coatings. To explore the apparent contradiction between experiment and practice, those conditions were examined which might lead to an in-situ lowering of the SEE yield. One such condition is electron-bombardment of the TiN-coated surfaces during initial running of rf devices.

2. Experiment

The experimental apparatus consisted of a stainless steel UHV analysis chamber linked to a process system chamber via a magnetically coupled sample transfer mechanism (Figure 1). The pressure was typically 2×10^{-10} Torr in the analysis chamber and 1×10^{-9} Torr in the process chamber.

A Vacuum Generators, Ltd. CLAM 100 XPS unit controlled by a Digital Equipment Corporation Model LSI-11 microcomputer was used to collect the Auger electron spectroscopy (AES) and X-ray photoelectron spectroscopy (XPS) data using electron pulse counting techniques. The total secondary electron emission (SEE) yield data were collected using an electron beam at normal incidence, a programmable high voltage power supply and an electrometer which were also under computer control (Figure 2).

The SEE measurements were done using a retarding voltage method[1] in which a 1.5 keV electron beam with a current of 2 nA (current density 4 μA-cm^{-2}) strikes the sample whose potential is varied from -50 to -1450 volts in 10 volt steps. The current flowing through the sample was measured at each retarding voltage by an electrometer, and the total secondary yield σ was calculated using:

$$\sigma = 1 - (\text{target current/primary current}) \tag{1}$$

The electron dose per yield curve was 1×10^{16} cm^{-2}.

The AES measurements were taken using an electron current of 50 nA rastered over approximately .25 cm^2 (current density 0.2 μA-cm^{-2}) of the sample. The analyzer was operated in the constant retard ratio (CRR, energy resolution $\sim$ 1%) mode for the AES measurements. The electron dose per AES curve was 1.4×10^{15} cm^{-2}.

The XPS data was collected using a Mg anode bombarded with 12 keV electrons at 20 mA. The Vacuum Generators, Ltd. analyzer was operated in

the constant analyzer energy (CAE, energy resolution $\sim$ 0.75 eV) mode with a pass energy of 20 eV. Photoelectrons were collected from .17 cm^2 sample area, chosen to fall within the area dosed in the electron beam exposure experiments to be described later. Binding energy references for XPS are the Pd Fermi edge (BE=0) and the Ag $3d_{5/2}$ core line (BE=368.2 eV). Photoelectron dose for a typical XPS spectrum was 1×10^{15} cm^{-2}.

The samples were single-crystal Nb discs of unknown orientation, 1.6 cm diameter $\times$ 0.5 cm thick, cut from low Ta (<350 ppm) rods which have been outgassed at 2500 K. After machining, they were mechanically polished with .5 μm diamond paste and electropolished in 10% HF – 90% H_2SO_4 solution which removed approximately 50 μm of Nb surface.

The discs were sputter-cleaned *in situ* and the various films were sputter-ion deposited using a Kaufman-type[3] ion source. The films were generally deposited to a thickness of 14 nm as determined by using a quartz-crystal thickness monitor, this being the thickness of the TiN coatings used successfully at SLAC. Immediately after deposition the samples were transferred to the analysis tank for the SEE, AES, and XPS measurements.

After the data on the as-deposited films was collected, the samples were moved to a loading chamber where they were exposed to room air (295K, 50% relative humidity) at atmospheric pressure for one hour. The loading chamber was then evacuated and the samples were transferred back to the analysis tank for characterization as described above.

The electron beam exposures were accomplished using an energy of 1067 eV and a current of $\sim$ 400 nA rastered over $\sim$1 cm^2 for the 140Å TiN and NbC and $\sim$ 80 nA rastered over 0.4 cm^2 for the 15Å TiN, 140Å NbN, 140Å TiC films and the oxidized uncoated Nb surface.

3. Results

When referring to Figures 3-20, (a) refers to the as-deposited films; (b) refers to the films exposed to air; and (c) refers to the results after electron beam bombardment. Data is also presented for the clean Nb substrate and its air-oxidized surface. Curves on the XPS and AES plots are offset vertically for clarity.

The SEE measurements indicate that the lowest σ occurs on the as-deposited films. In some cases σ remains ≤ 1 over the entire incident energy range 50-1450 eV. After exposure to air, σ rises substantially above the initial value. Subsequent electron beam bombardment serves to reduce σ, in some cases to nearly the value obtained for the as-deposited film.

The AES measurements of the as-deposited films show the elemental compositions of the surfaces of the films. In addition to the primary elements of the deposited materials small amounts of oxygen are seen on some of the layers. This is probably due to H_2O desorption from the chamber walls during sputter deposition. After exposure to air, an increase in the oxygen peak area is noted along with a small increase in the carbon level. Changes in the structure of the primary AES peaks can reflect changes in the chemical composition of surface layers in our data. After electron beam bombardment, however, only small changes in the AES spectra are seen, compared to the oxidized overlayers, indicating that the relative amounts and chemistry of each element is largely unaffected. Retrieving information about chemical states is difficult due to the nature of the AES technique and quantitative chemical analysis of these spectra was therefore not undertaken.

The XPS data gives more easily extractable information about the chemical states present in the films but probes to a somewhat greater depth than AES. After deposition, XPS shows primarily the material sputtered onto the Nb discs, with some films incorporating small amounts of oxides (again, probably due to H_2O desorbed from the chamber walls during sputter deposition). After exposure

to air the amount of oxide present in each material rises significantly with a concomitant decrease in the primary species. After electron bombardment, XPS shows that the oxide levels are slightly reduced by bombardment.

In addition to XPS, AES and SEE, we have made some electron-induced-desorption (EID) measurements of the oxidized layers on Nb and NbN/Nb. O^+ emission is observed whose desorption rate increases with e-beam exposure, in agreement with the observations of others[4]. This rate increase is due to a rise in the surface concentration of weakly-bound surface oxygen, created during reduction of the Nb_2O_5 to sub-oxides by electron bombardment.

4. Discussion

4.1 Nb

The results presented here for clean sputtered Nb (Figures 3-5) are similar to those which we have obtained for furnace-cleaned Nb (2300K, 21 hrs. at 4×10^{-10} mbar). Sputtered surfaces can be made essentially C and O-free whereas we have observed small amounts (<5% of a monolayer) of O on all furnace-cleaned samples. This appears to be due to dissolved O from the bulk diffusing to the surface during furnace heating. For both types of cleaning, however, we obtained essentially identical XPS, AES, and SEE data in all other respects.

The yield (Figure 3a) of the sputter-cleaned Nb surface displays an unusual shape compared to the oxidized surface and overlayers. There is also structure evident in the curve which is not due to electronic noise (noise is evident in Figures 3b and 3c). Moreover, the structures are more emphasized in yield measurements made on furnace-cleaned samples. These structures are due to the single crystal nature of the sample used and we have not observed them in polycrystalline samples where the yield shapes are similar to Figure 3b and 3c. These structures are caused by Bragg reflections at energy gaps in the conduction band structure and have been observed before in Fe[5,6] This view is supported by the change in

shape and structure brought about by the oxidation process. Room temperature oxidation of Nb is known to result in mixed oxides[8,9] and the oxide layers are also rather inhomogeneous structurally so that the single crystal nature of the original surface is not preserved.

The XPS spectrum for clean Nb (Figure 4a) is similar to that previously reported[10] for sputter-cleaned surfaces. The oxidized spectrum (Figure 4b) shows the usual presence of Nb_2O_5 (207.5 eV) and other oxides (broadening between the peaks) as well as metallic Nb within the XPS detected layer. By curve fitting[11] Figures 4a and 4b, the thicknesses of the Nb oxide overlayer was determined to be 1.65 nm. This thickness is in fair agreement with results by Grundner and Halbritter[8] for furnace-cleaned Nb exposed for 0.5 hr in air, giving an Nb oxide thickness of $\leq$2 nm, but long cooling in the furnace (10^{-8} mbar, 50 hrs) probably led to some oxide growth prior to air exposure.

Electron-bombardment results for all samples are discussed separately in Sect. 4.6.

4.2 TiN

Yield results for as-deposited 1.5nm (Figure 6(a)) and 14 nm (Figure 9(a)) TiN coatings are substantially the same, although there is a hint of the crystalline Nb substrate effect (discussed above) present in the curve for 1.5 nm TiN (compare Figure 6(a) and 3(a)). After oxidation, the yield is higher for that of the thinner TiN layer, probably because of enhanced backscatter from the Nb substrate in the 1.5 nm layer case as compared to the backscatter from the underlying lower atomic number TiN in the 14 nm case. The XPS curve of Figure 7(b) shows that the 1.5 nm layer was almost completely converted to TiO_2[11]. Some oxidation of the Nb substrate is evident as well. The underlying Nb substrate of the 14 nm TiN film could not be seen because the electron attenuation length was much smaller than the TiN film thickness, but the Ti spectrum (Figure 10(b)) does show considerable nitride signal from un-oxidized TiN within the detected

layer. In a previous publication we have shown that TiN oxidizes to TiO_2 with a Ti_2O_3/Ti-oxynitride interface between the TiN and TiO_2[11]. That result has also been reported in other recent work[12] on TiN.

4.3 TiC

The results (Figures 12-14) for the as-deposited and oxidized surfaces of this material are very similar to that of TiN (at the same thickness). The backscatter contribution to the yield at higher primary energy is the same as well. The amount of oxidation appears less (Figure 13(b)) than in the TiN case (Figure 10(b)) although TiO_2 is clearly evident and, because the yield rises to that of oxidized TiN (Figures 9(b) and 12(b)), the oxide is apparently thick enough to produce the increased yield. In fact, the AES results (Figures 11(b) and 14(b)) for the amount of oxygen present show equality there.

4.4 NbN

The yield (Figure 15) for NbN is slightly higher than that for Nb for as-deposited and oxidized. The oxidation produces predominantly Nb_2O_5 (Figure 16(b)) as in the case of Nb oxidation. The hope is that, since NbN has a rather high superconducting transition temperature (T_C=16K), the oxide might be fine-grained as opposed to the native Nb_2O_5/Nb oxide which is known[8] to be very inhomogeneous. We have not investigated the granularity of our films but it is clear that the yield for NbN is similar to Nb, thus making further investigations worthwhile. The Nb_2O_5 layer on NbN is reported to grow more slowly than that on Nb and saturates at a lower thickness than Nb, although there is evidence that it, too, may be fragmented[13].

4.5 NbC

Like TiC, NbC does not show much oxidation in XPS (Figure 19(b)) but again its oxidized yield is rather high and the as-deposited yield is the highest of the metalloids tested.

XPS peak positions in eV and peak area ratios for Nb and the metalloids are summarized in Tables I and II and compared to literature values where they are available.

Using transition metal carbide and nitride overlayers as secondary electron suppressors on Nb would seem to be an ideal choice. They are excellent electrical conductors, have low secondary emission coefficients[1] and high superconducting transition temperatures. From the data (Figures 6,9,12,15,18, all (a)), σ is quite low for as-deposited overlayers on Nb and the electron backscatter contribution at higher primary energy is smaller than that for uncoated Nb (compare for example, σ for clean Nb and 14 nm TiN/Nb. At this time, the mechanism for reduced secondary emission in transition metal carbides and nitrides is not understood, but presumably the secondary electron attenuation caused by electron-electron scattering is similar to that of metals.

Upon exposure to air (and pure oxygen, as well, we have found), the bare Nb surface and its overlayers form thin surface oxides at the exposures used in this experiment. XPS shows the presence of Nb_2O_5 (as well as sub-oxides) for oxidized Nb, NbN and NbC. TiO_2 is observed for TiN and TiC oxidized overlayers. AES (which probes a shallower depth) confirms these observations. XPS measurements[11] of the oxidation of TiN layers on alumina yield a TiO_2 thickness of 0.9 nm, consistent with the results of our oxidized TiN measurements here.

The SEE yield of our samples shows a substantial increase upon oxidation. Enhanced yields for thin oxides, on Nb for example, have been observed before[8]. Such increases are due to the reduced electron-electron scattering mechanism in

insulators. The primary beam penetration depth, as well, is larger in the metal oxide than in the parent metal. For example in oxidized Nb, where the peak of the SEE yield is $\sim$ 300 eV (Figure 3), the penetration depth[18] at that energy is 3.4 nm for Nb and 5.6 nm for Nb_2O_5. If the penetration depth is roughly the oxide thickness, the yield will be enhanced compared to either substantially deeper or shallower penetration[19]. The fact that our oxidized Nb overlayer thickness is about one-third of this penetration depth suggests that primary electron backscatter from the Nb substrate strongly enhances the secondary yield.

Charging of the oxide layer under electron bombardment has been observed in thin MgO layers[20] and oxidized Nb[8] but we see no evidence of that here, although we have seen charging in thick oxides and on severely contaminated surfaces.

4.6 ELECTRON-BOMBARDMENT

Extensive electron-bombardment of the oxidized Nb and oxidized overlayers produces damage in the form of broken bonds, reduced oxides, excited species, mobile and immobile holes, etc. An examination of the electron-bombardment results in Figures 3-20 shows that the SEE yield coefficient is much more sensitive to the damage induced by the bombardment than are either XPS or AES. The electron-desorbed O^+ (and possibly neutral CO and CO_2) observed in the EID results described earlier is seen as a very small change in the XPS and AES spectra. Also, there is only minimal evidence (see, e.g., Figures 16b,c) in XPS for reduction of the oxidized surface as a result of bombardment. One can begin to detect the onset of a shoulder at the lower binding energy side of the metal-oxide peak which might be ascribed to lower oxides being formed.

At the same time, large changes are occurring in the SEE yield. Figures 21-26 are plots of the yield as a function of bombardment exposure. The exposure measurements were made subsequent to the σ, XPS and AES analyses and, as such, the dose in Figures 21-26 is additional to the dose received during those

analyses. Changes are clearly visible at the 1 x 10^{-4} C-cm^{-2} level (e.g. in NbN), five times lower than that observed previously in AES for beam damage in very sensitive systems, condensed multilayers of $(CH_3)_2O$, CH_3OH and H_2O[21].

The damage threshold crossection, Q, can be obtained from Figures 21-26 via the first order rate equation[22]:

$$\sigma = \sigma_o \exp(-DQ/\epsilon) \tag{2}$$

where σ_o is the yield prior to bombardment, D is the electron dose in C-cm^{-2}, Q is the crossection in cm^2 and ϵ is the electronic charge in coulombs. The results for Q are: oxidized Nb - 1.1×10^{-19} cm^2, 1.5 nm TiN - 6.3×10^{-19} cm^2, 14 nm TiN - 5.4×10^{-19} cm^2, TiC - 7.0×10^{-19} cm^2, NbN - 1.0×10^{-18} cm^2 and NbC - 2.9×10^{-19} cm^2. These crossections are somewhat smaller than those typically associated with dissociative ionization of adsorbed molecules (10^{-16} - 10^{-18} cm^2).

"Maximal valency" oxides (such as SiO_2, TiO_2 and Nb_2O_5) decompose easily under electron bombardment[23]. The damage introduced apparently causes strong electron scattering which is detectable in the SEE yield well before changes in oxide states appear in the XPS or AES. It's not expected that there is a yield dependence on the oxide states themselves, according to work on powdered oxides of Nb[1].

5. Conclusions

Although clean Nb has a SEE yield low enough to be useful for the construction of RF cavities, the native oxide which forms upon exposure to air increases the SEE yield enough to cause multipacting to be a major problem. It is therefore useful to coat Nb structures with materials capable of reducing the effects of multipacting, and which preserve the superconducting properties of the clean Nb surface.

Materials such as NbC, NbN, TiC and TiN, as-deposited, have SEE yields low enough to minimize multipacting effects. Exposing these coatings to air causes a rise in the SEE yields and would apparently make them unsuitable for use in RF cavities.

We have shown, however, that electron bombardment with doses of less than 10^{18} cm^{-2} reduces the SEE yields to values approaching those of the as-deposited films. We conclude that the in-situ electron bombardment, which occurs during rf device processing and is several orders of magnitude greater than that used in our experiments, serves to reduce the effective SEE yield and thereby may cause substantial reduction in multipacting in coated rf cavities.

References

1. E.L. Garwin, E.W. Hoyt, R.E. Kirby and T. Momose, J. Appl. Phys., 59, 3245 (1986).
2. L.E. Toth, Transition Metal Carbides and Nitrides, Academic Press, N.Y. 1972.
3. P.D. Reader and H.R. Kaufman, J. Vac. Sci. Technol. 12, 1344 (1975).
4. T.T. Lin and D. Lichtman, J. Mat. Sci. 14, 445 (1979).
5. E. Kisker, R.E. Kirby, E.L. Garwin, F.K. King, E. Tamura and R. Feder, J. Appl. Phys. 57, 3021 (1985).
6. E. Tamura, R. Feder, J. Krewer, R.E. Kirby, E. Kisker, E.L. Garwin and F.K, King, Sol. State Comm. 55, 543 (1985).
7. S. Hoffman and J.M. Sanz, J. Trace and Microprobe Techniques, 1, 213 (1982-83).
8. M. Grudner and J. Halbritter, J. Appl. Phys. 51, 397 (1980).
9. M. Grundner and J. Halbritter, Surface Sci. 136, 144 (1984).
10. J. Kwo, G.K. Wertheim, M. Gurvitch and D.N.E. Buchanan, Appl. Phys. Lett. 40, 675 (1986).
11. A.R. Nyaiesh, E.L. Garwin, F.K, King and R.E. Kirby, J. Vac. Sci. Technol., Sept/Oct, 1986.
12. C. Ernsberger, J. Nickerson, A.E. Miller and J. Moulder, J. Vac. Sci. A3, 2415 (1985).
13. A. Ermolieff, M. Girard and C. Raoul, Appl. Surf. Sci. 21, 65 (1985).
14. L. Ramquist, K. Hamrin, G. Johansson, A. Fahlman and C. Nordling, J. Phys. Chem. Solids 30, 1835 (1969).
15. L. Ramquist, K. Hamrin, G. Johansson, U. Gelius and C. Nordling, J. Phys. Chem. Solids 31, 2669 (1970).

16. H. Höchst, R.D. Bringans, P.S. Steiner and T. Wolf, Phys. Rev. B 25, 7183 (1982).

17. L. Porte, M. Demosthenons and T.M. Duc, J. Less Comm. Met. 56, 183 (1977).

18. M. Grunder and J. Halbritter, J. Appl. Phys. 51, 5396 (1980).

19. O.C. Wells, Scanning Electron Microscopy, McGraw-Hill, New York, 1974.

20. J.W. Gibson and R.E. Thomas, Applic. Surf. Sci. 14, 56 (1982-83).

21. P.H. Holloway, T.E. Madey, C.T. Campbell, R.R. Rye and J.E. Houston, Surface Sci., 88, 121 (1979).

22. C.G. Pantano and T.E. Madey, Applic. of Surface Sci., 7, 115 (1981).

23. M.L. Knotek and P.J. Feibelman, Surface Sci. 90, 78 (1979).

Table I XPS Peak Positions*, eV

As Deposited

	Nb $3d_{5/2}$	Ti $2p_{3/2}$	C 1s	N 1s
Nb	202.2(202.0[7])			
NbN	203.2(203.4[13])			397.6
NbC	203.6(203.4[15])		282.8(282.1[15])	
TiC		454.8(454.8[14])	281.9(281.7[14])	
TiN		454.9(455.1[16])		397.2(397.4[16])

Oxidized

	Nb $3d_{5/2}$	Ti $2p_{3/2}$	O 1s
Nb	207.5(207.4[7])		531.0
NbN	207.1(206.9[13])		530.5
NbC	206.9		530.5
TiC		458.6	530.3
TiN		458.4(458.9[17])+	530.3(530.4[17])+

* Literature results in parentheses, adjusted to Ag $3d_{5/2}$=368.2 eV, Au $4f_{7/2}$ = 84.0 eV or adventitious carbon at 285.0 eV.

+ Reference 17 values are for TiO_2.

Table II XPS Peak Area Ratios, As Deposited

NbN: Nb $3d_{5/2}$ / N 1s=10.25

NbC: Nb $3d_{5/2}$ / C 1s=12.33

TiC: Ti $2p_{3/2}$ / C 1s= 8.78

TiN: Ti $2p_{3/2}$ / N 1s= 3.14

Figure Captions

1. Coupled surface analysis-process systems. The volume of each chamber is ~100 liters. Symbols are American Vacuum Society standard. Other acronyms: EID - electron induced desorption, SIMS - secondary ion mass spectrometry, AES - Auger electron spectroscopy, XPS - x-ray photoelectron spectroscopy, SEE - secondary electron emission, SAM - scanning Auger microscopy, RGA - residual gas analyzer, E-B Heat - electron beam impact heating.

2. Total secondary electron emission yield measurement schematic. A measured curve of 0-1500 eV takes ~400 sec using 10 eV steps, one second settling time between points and 200 reads are averaged per point. During this time the primary beam current varies $< 1\%$. I_T - target current, I_P - primary current, I_{SE} - secondary electron current.

3. Total secondary electron emission yield vs. primary electron energy for sputter-cleaned Nb. a) As cleaned, b) exposed to room air 1 hr., c) electron-bombarded, dose rate = 1.58×10^{12} cm^{-2}-sec^{-1} and total dose = 6.1×10^{17} cm^{-2}.

4. XPS spectra for sputter-cleaned Nb. a) As cleaned, b) exposed to room air 1 hr., c) electron-bombarded, same rate and dose as Fig. 3. M - metal, O - oxide. Spectra offset vertically for clarity.

5. AES spectra for sputter-cleaned Nb. a) As cleaned, b) exposed to room air 1 hr., c) electron-bombarded, same rate and dose as Fig. 3. Spectra offset vertically for clarity.

6. Total secondary electron emission yield vs. primary electron energy for 1.5 nm TiN layer on Nb. a) As deposited, b) exposed to room air 1 hr., c) electron-bombarded, dose rate = 1.61×10^{12} cm^{-2}-sec^{-1} and total dose = 1.7×10^{17} cm^{-2}.

7. XPS spectra for 1.5 nm TiN layer on Nb. a) As deposited, b) exposed to

room air 1 hr., c) electron-bombarded, same rate and dose as Fig. 6. N - nitride, O - oxide. Spectra offset vertically for clarity.

8. AES spectra for 1.5 nm TiN layer on Nb. a) As deposited, b) exposed to room air 1 hr., c) electron-bombarded, same rate and dose as Fig. 6. Spectra offset vertically for clarity.

9. Total secondary electron emission yield vs. primary electron energy for 14 nm TiN layer on Nb. a) As deposited, b) exposed to room air 1 hr., c) electron-bombarded, dose rate = 2.45×10^{12} cm^{-2}-sec^{-1} and total dose = 8.1×10^{17} cm^{-2}.

10. XPS spectra for 14 nm TiN layer on Nb. a) As deposited, b) exposed to room air 1 hr., c) electron-bombarded, same rate and dose as Fig. 9. N-nitride, O-oxide. Spectra offset vertically for clarity.

11. AES spectra for 14 nm TiN layer on Nb. a) As deposited, b) exposed to room air 1 hr., c) electron-bombarded, same rate and dose as Fig. 9. Spectra offset vertically for clarity.

12. Total secondary electron emission yield vs. primary electron energy for 14 nm TiC on Nb. a) As deposited, b) exposed to air 1 hr., c) electron-bombarded, dose rate = 1.32×10^{12} cm^{-2}-sec^{-1} and total dose = $1.99 \times 10^{17} cm^{-2}$.

13. XPS spectra for 14 nm TiC layer on Nb. a) As deposited, b) exposed to room air 1 hr., c) electron-bombarded, same rate and dose as Fig. 12. C-carbide, O-oxide. Spectra offset vertically for clarity.

14. AES spectra for 14 nm TiC layer on Nb. a) As deposited, b) exposed to room air 1 hr., c) electron-bombarded, same rate and dose as Fig. 12. Spectra offset vertically for clarity.

15. Total secondary electron emission yield vs. primary electron energy for 14 nm NbN layer on Nb. a) As deposited, b) exposed to room air 1 hr., c)

electron-bombarded, dose rate = 1.31×10^{12} cm^{-2}-sec^{-1} and total dose = 1.7×10^{17}cm^{-2}.

16. XPS spectra for 14 nm NbN layer on Nb. a) As deposited, b) exposed to room air 1 hr., c) electron-bombarded, same rate and dose as Fig. 15. Spectra offset vertically for clarity.

17. AES for 14 nm NbN layer on Nb. a) As deposited, b) exposed to room air 1 hr., c) electron-bombarded, same rate and dose as Fig. 15. N-nitride, O-oxide. Spectra offset vertically for clarity.

18. Total secondary electron emission yield vs. primary electron energy for 14 nm NbC layer on Nb. a) As deposited, b) exposed to room air 1 hr., c) electron-bombarded, dose rate = 2.45×10^{12} cm^{-2}-sec^{-1} and total dose = 3.25×10^{17} cm^{-2}.

19. XPS spectra for 14 nm NbC layer on Nb. a) As deposited, b) exposed to room air 1 hr., c) electron-bombarded, same rate and dose as Fig. 18. C-carbide, O-oxide. Spectra offset vertically for clarity.

20. AES spectra for 14 nm NbC layer on Nb. a) As deposited, b) exposed to room air 1 hr., c) electron-bombarded, same rate and dose as Fig. 18. Spectra offset vertically for clarity.

21. SEE yield vs. electron bombardment exposure dose, 1067 eV, 200 nA-cm^{-2}, air-oxidized sputter-cleaned Nb.

22. SEE yield vs. electron bombardment exposure dose, 1067 eV, 200 nA-cm^{-2}, air-oxidized 1.5 nm TiN/Nb.

23. SEE yield vs. electron bombardment exposure dose, 1067 eV, 400 nA-cm^{-2}, air-oxidized 14 nm TiN/Nb.

24. SEE yield vs. electron bombardment exposure dose, 1067 eV, 200 nA-cm^{-2}, air-oxidized 14 nm TiC/Nb.

25. SEE yield vs. electron bombardment exposure dose, 1067 eV, 200 nA-cm^{-2}, air oxidized 14 nm NbN/Nb.

26. SEE yield vs. electron bombardment exposure dose, 1067 eV, 400 nA-cm^{-2}, air oxidized 14 nm NbC/Nb.

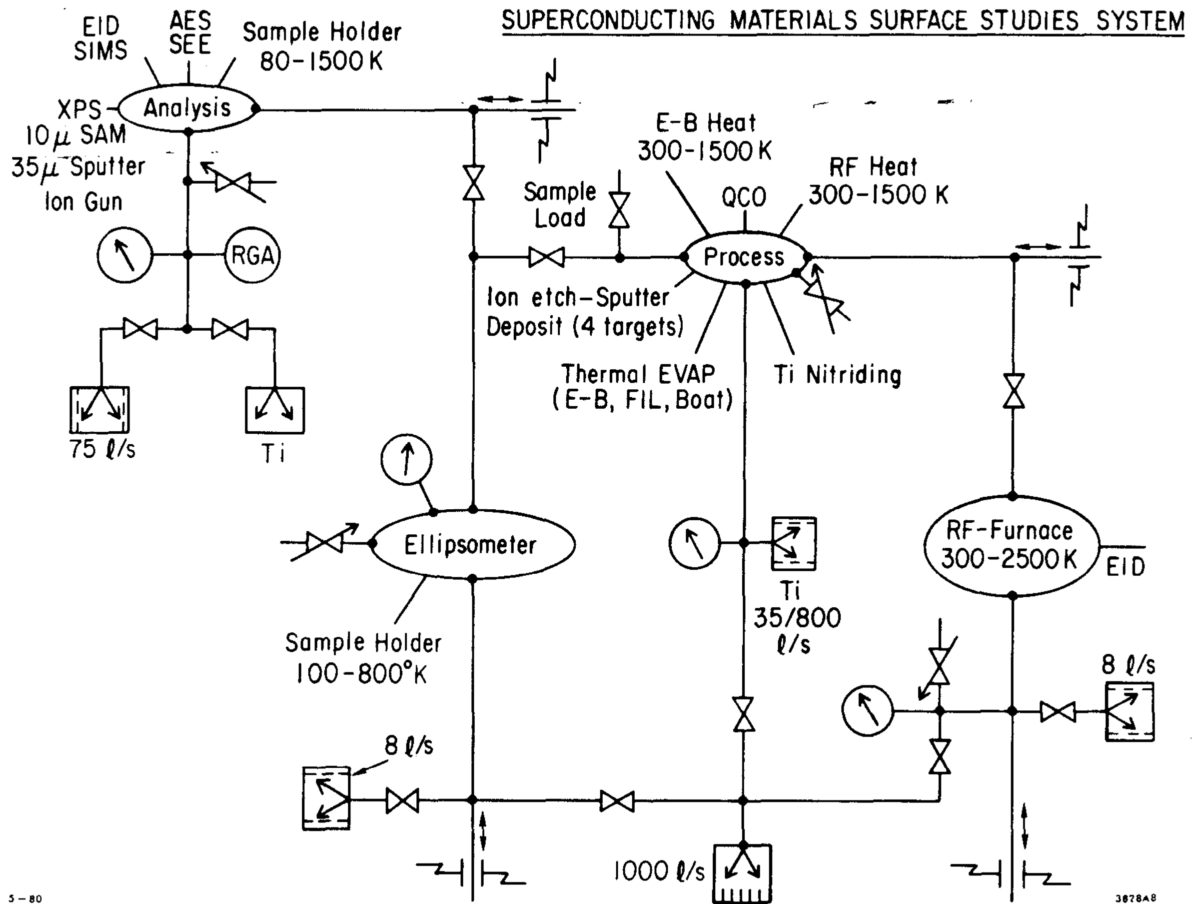

Fig. 1

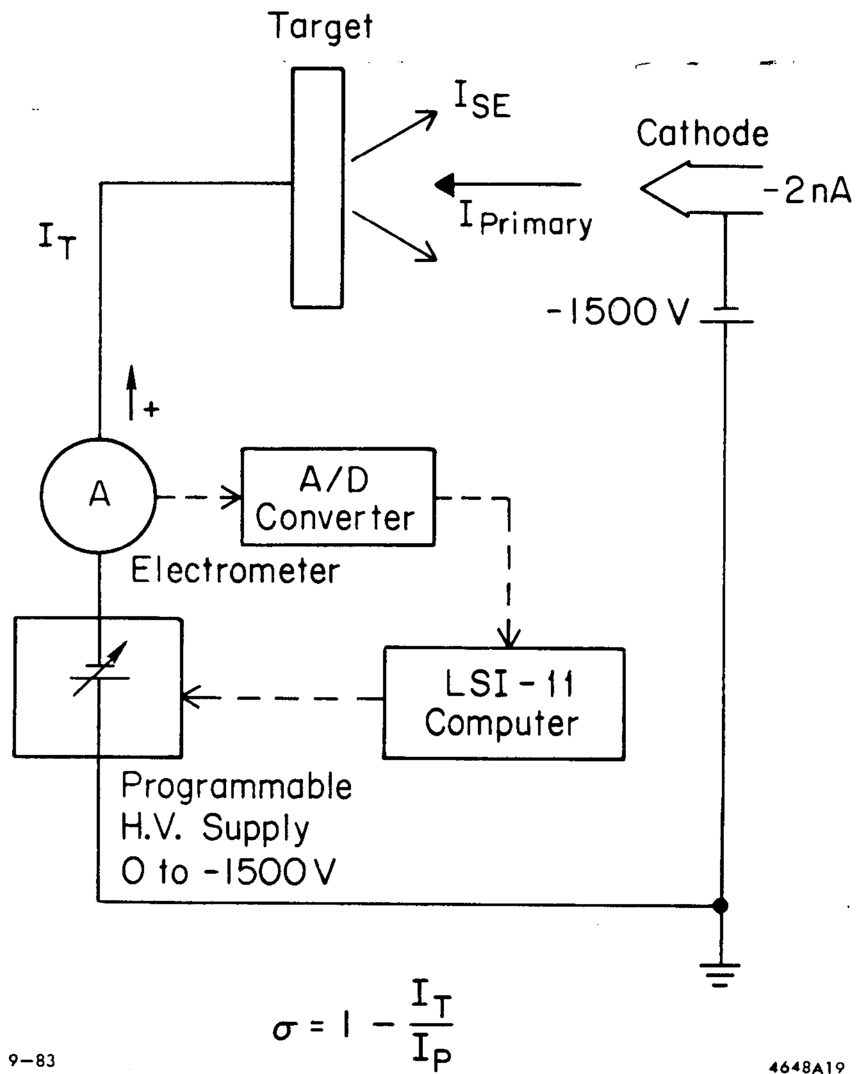

Fig. 2

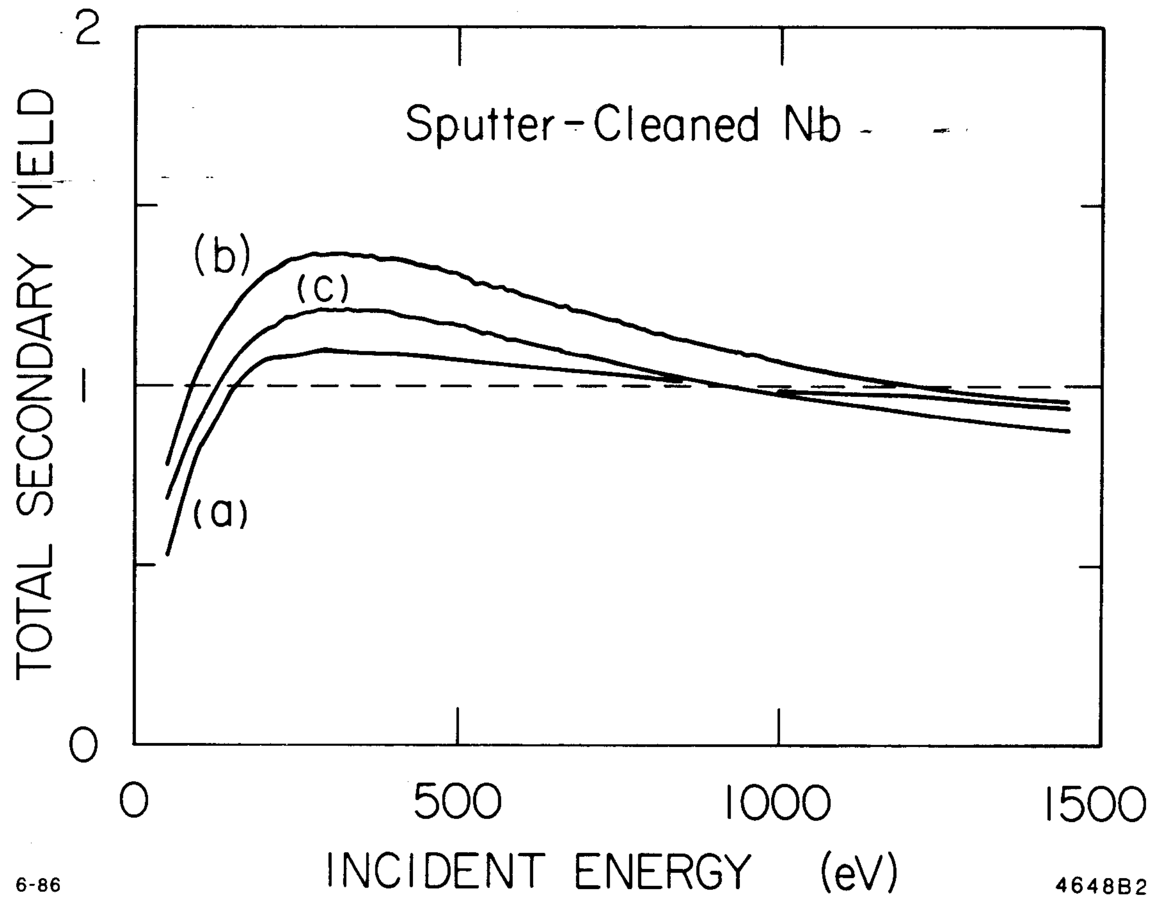

Fig. 3

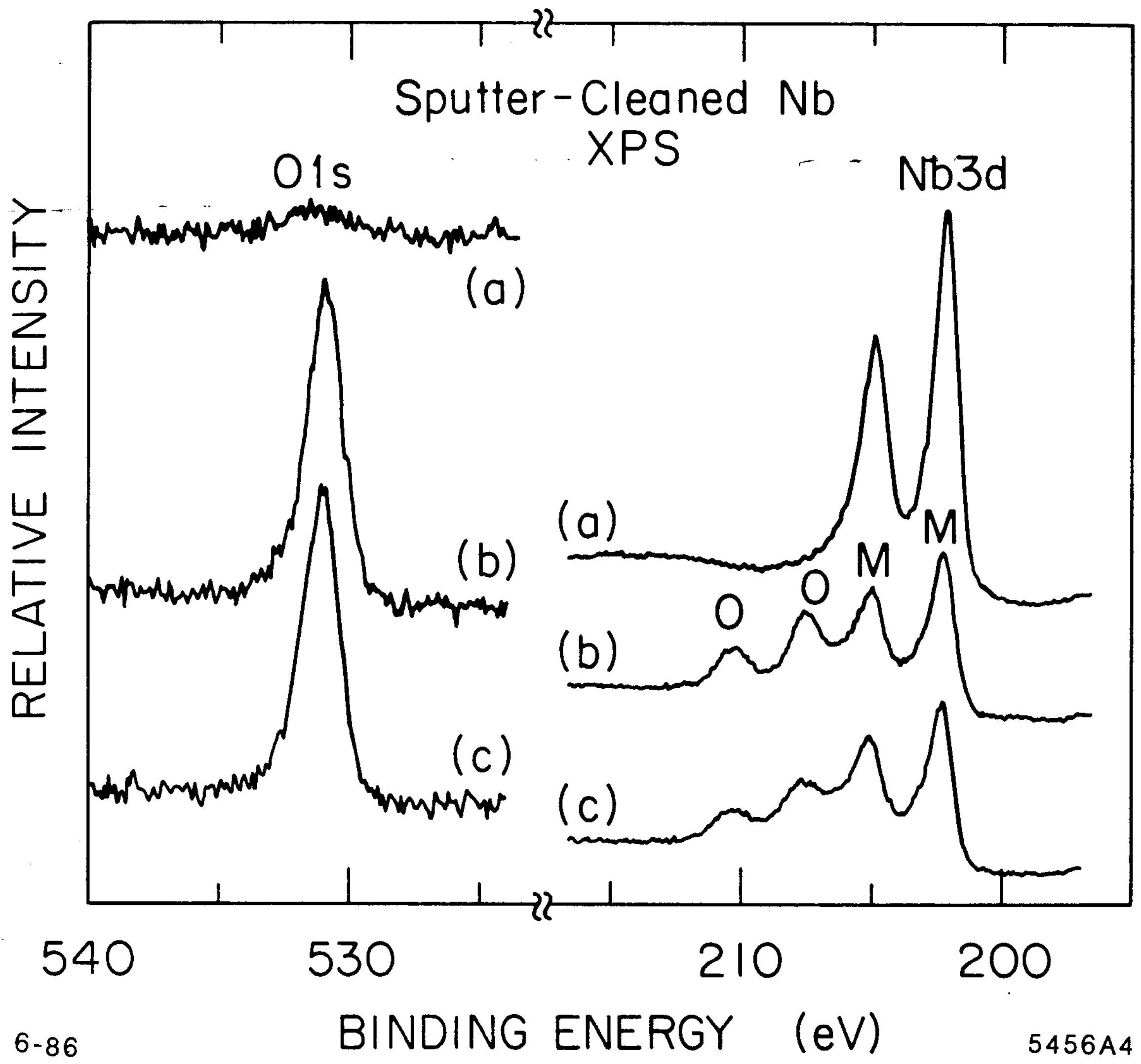

Fig. 4

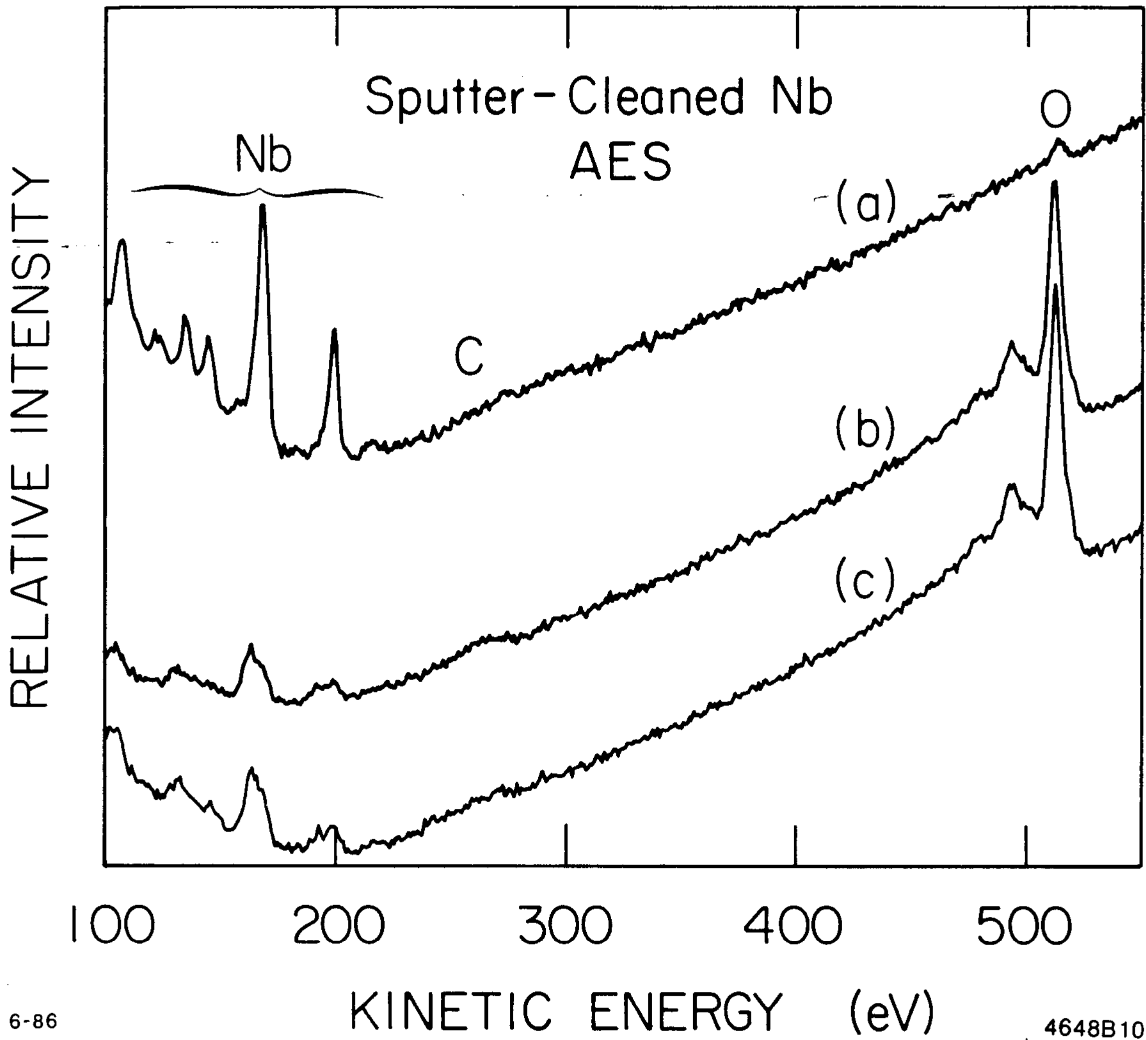

Fig. 5

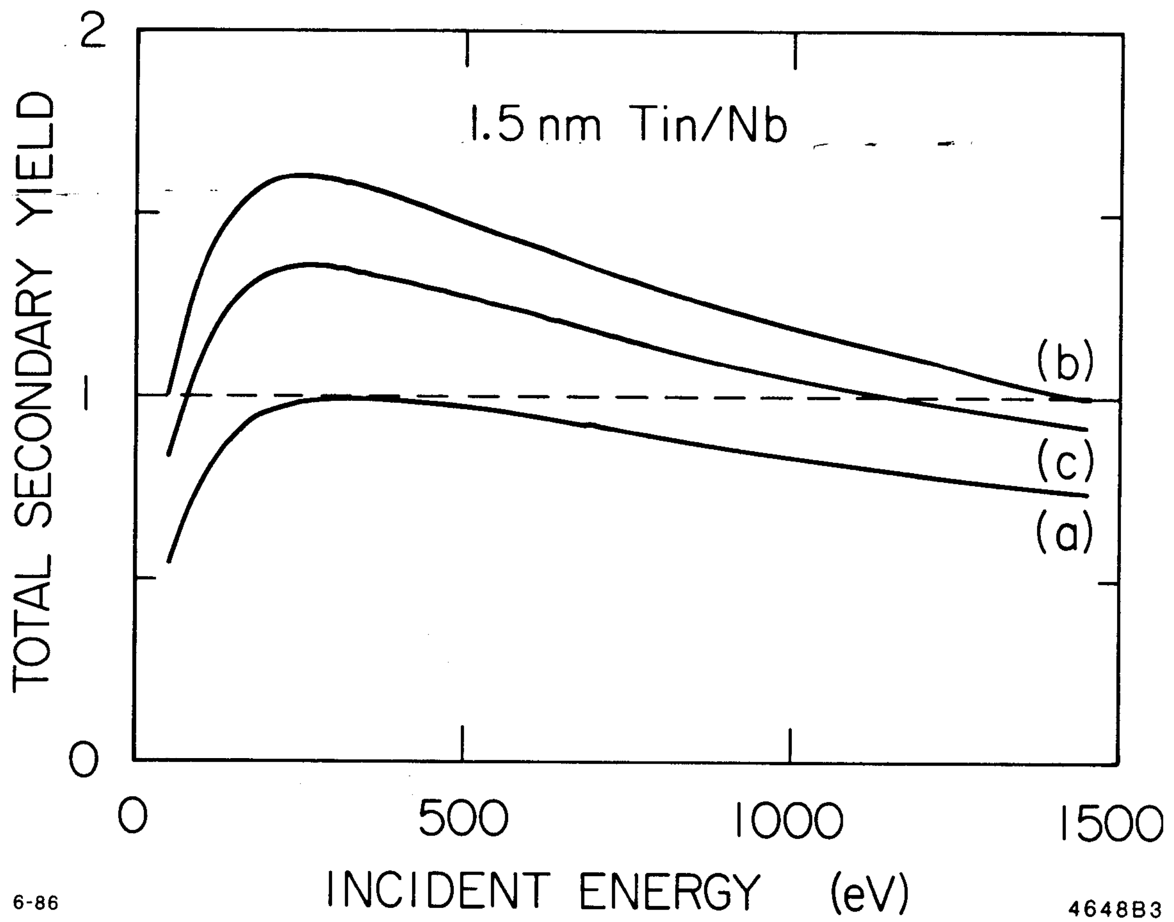

Fig. 6

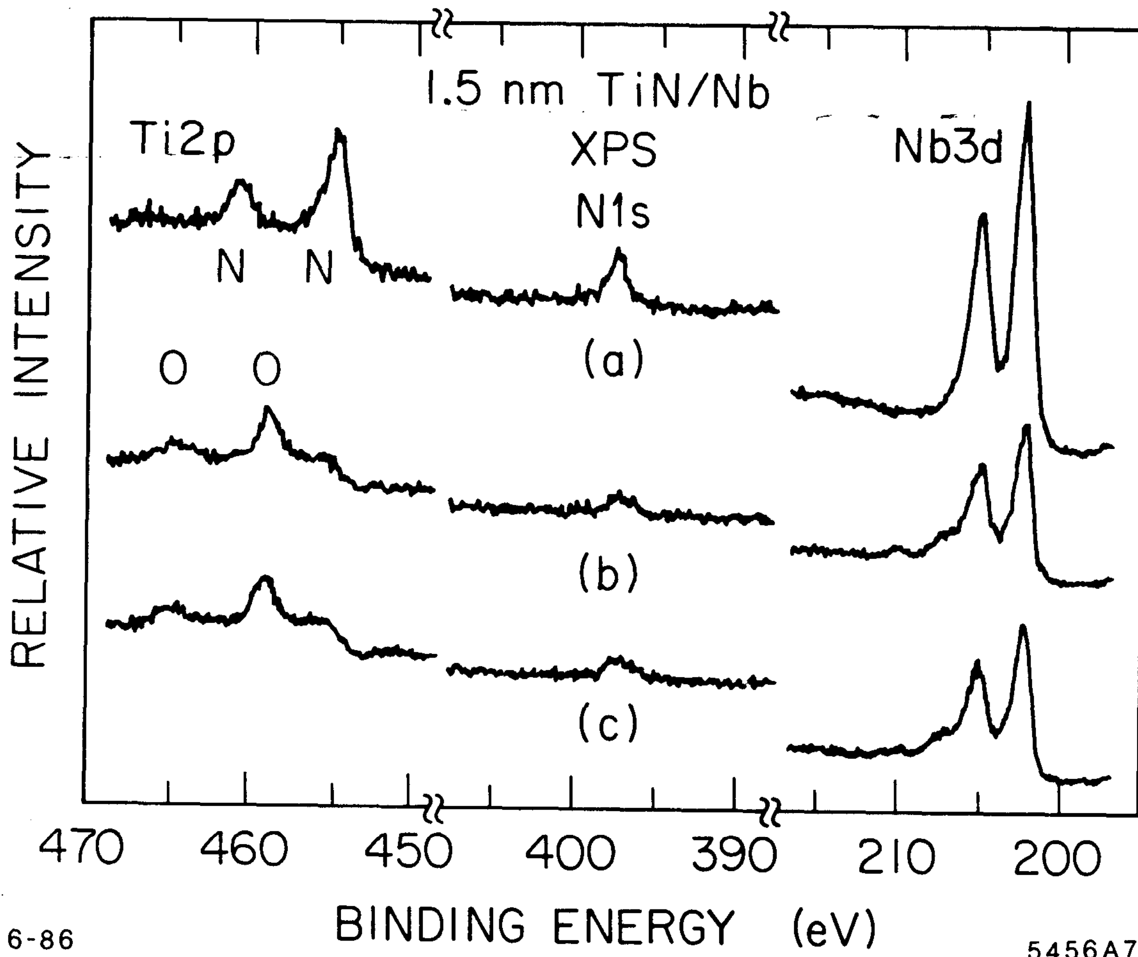

Fig. 7

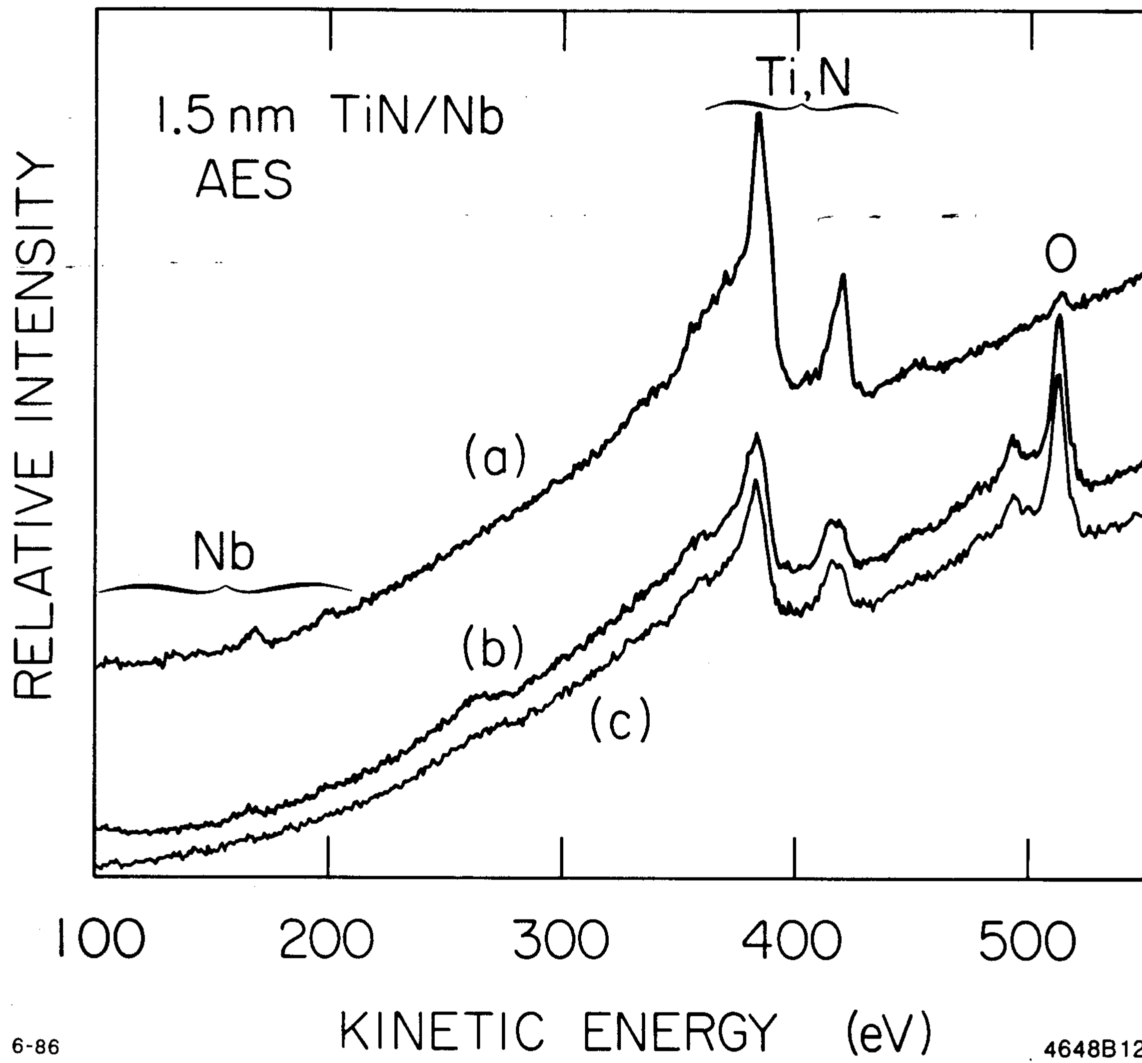

Fig. 8

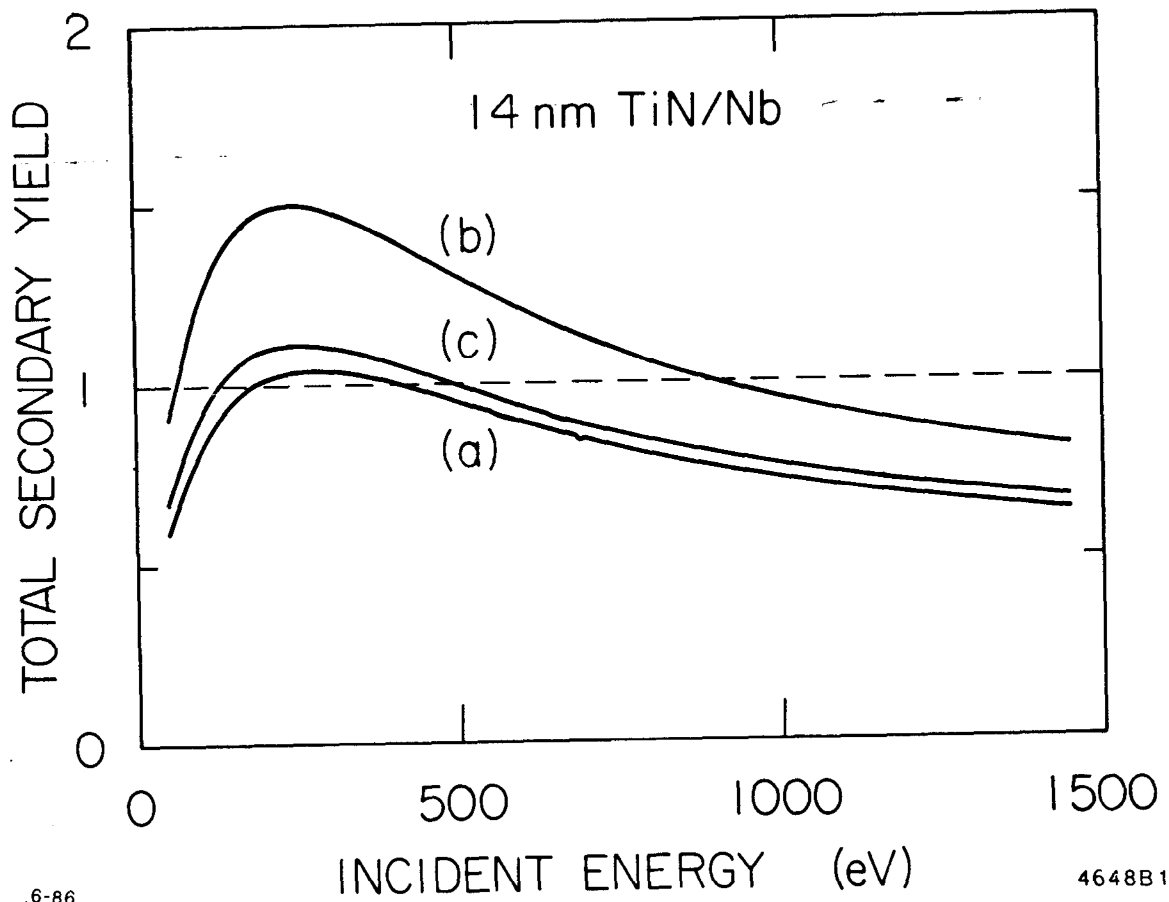

Fig. 9

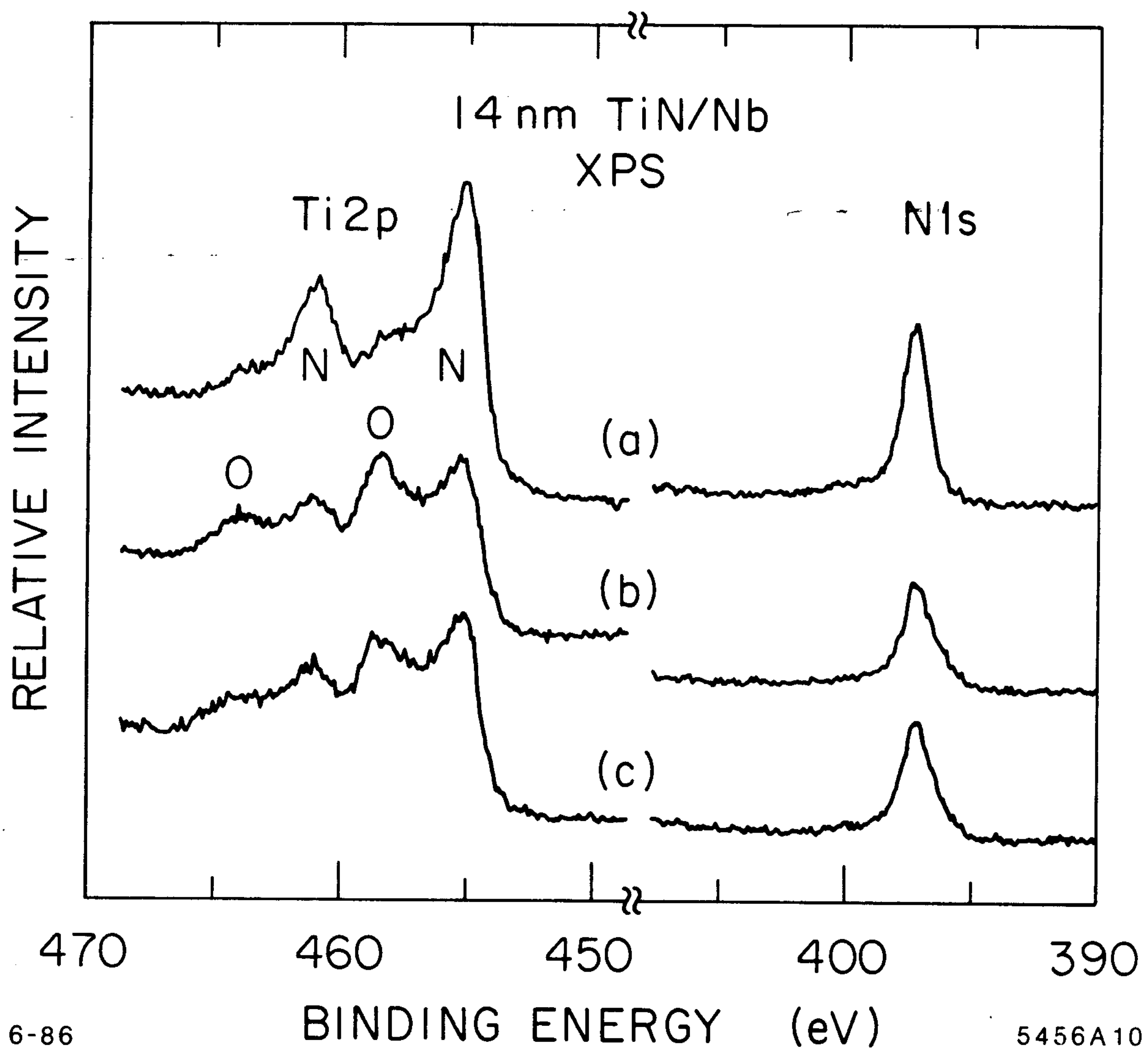

Fig. 10

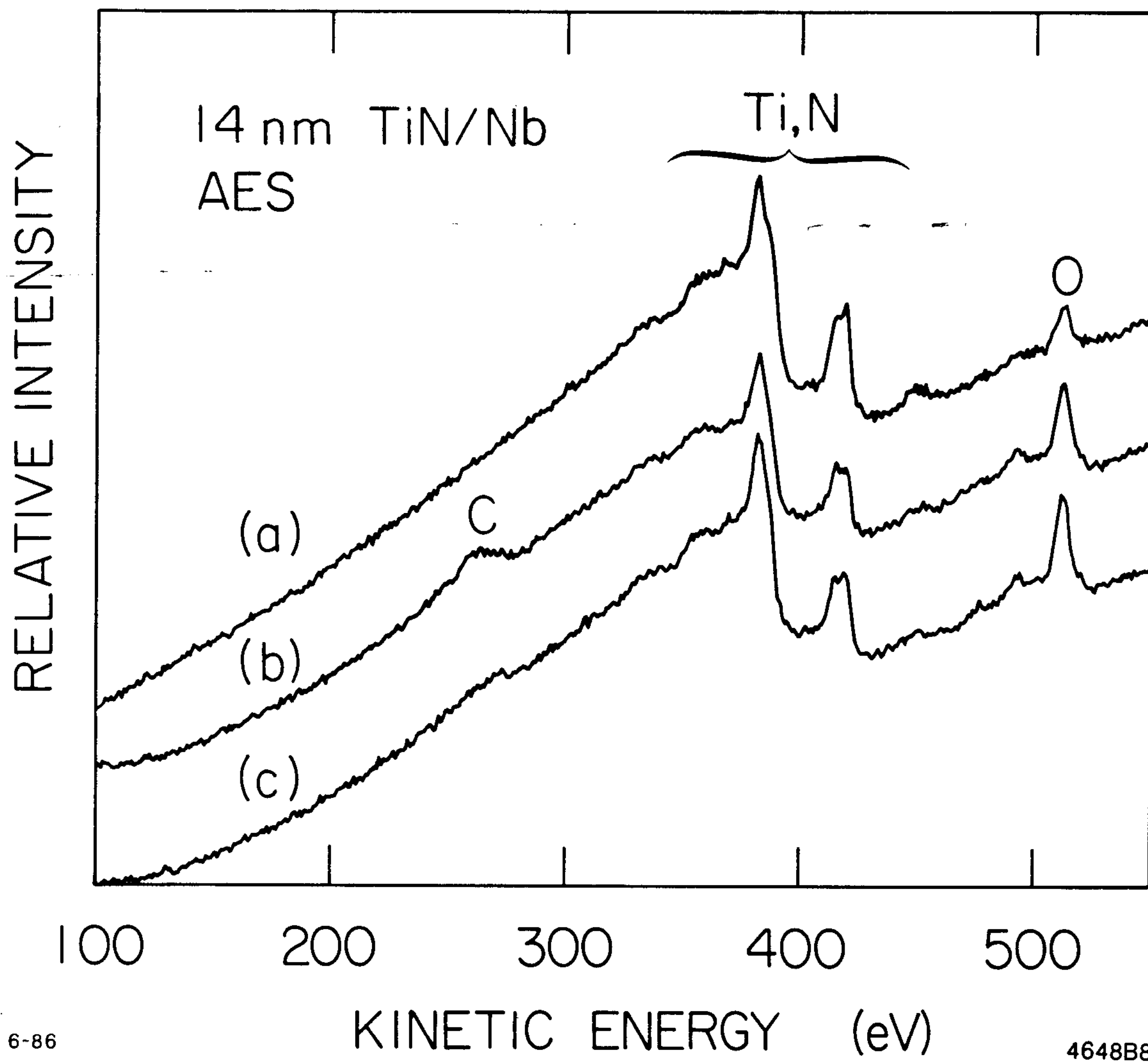

Fig. 11

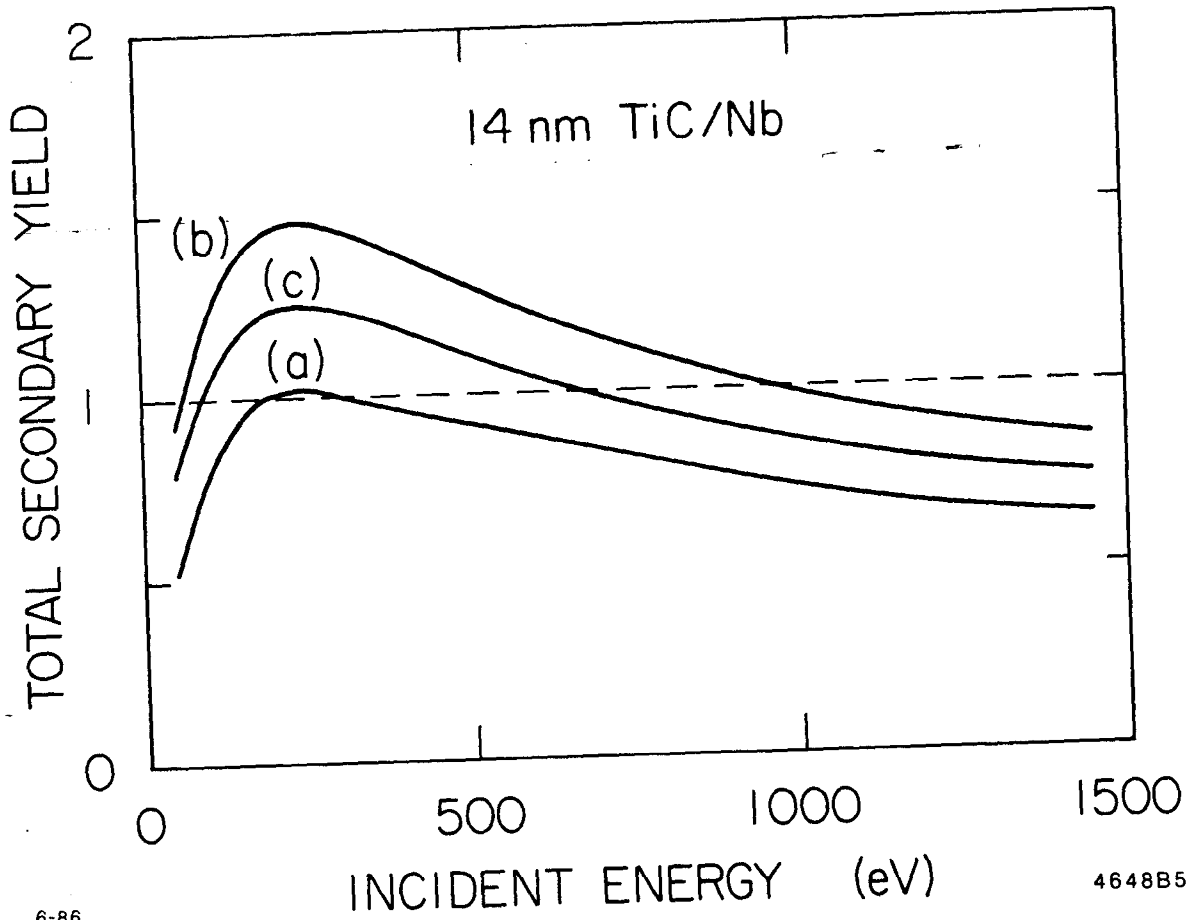

Fig. 12

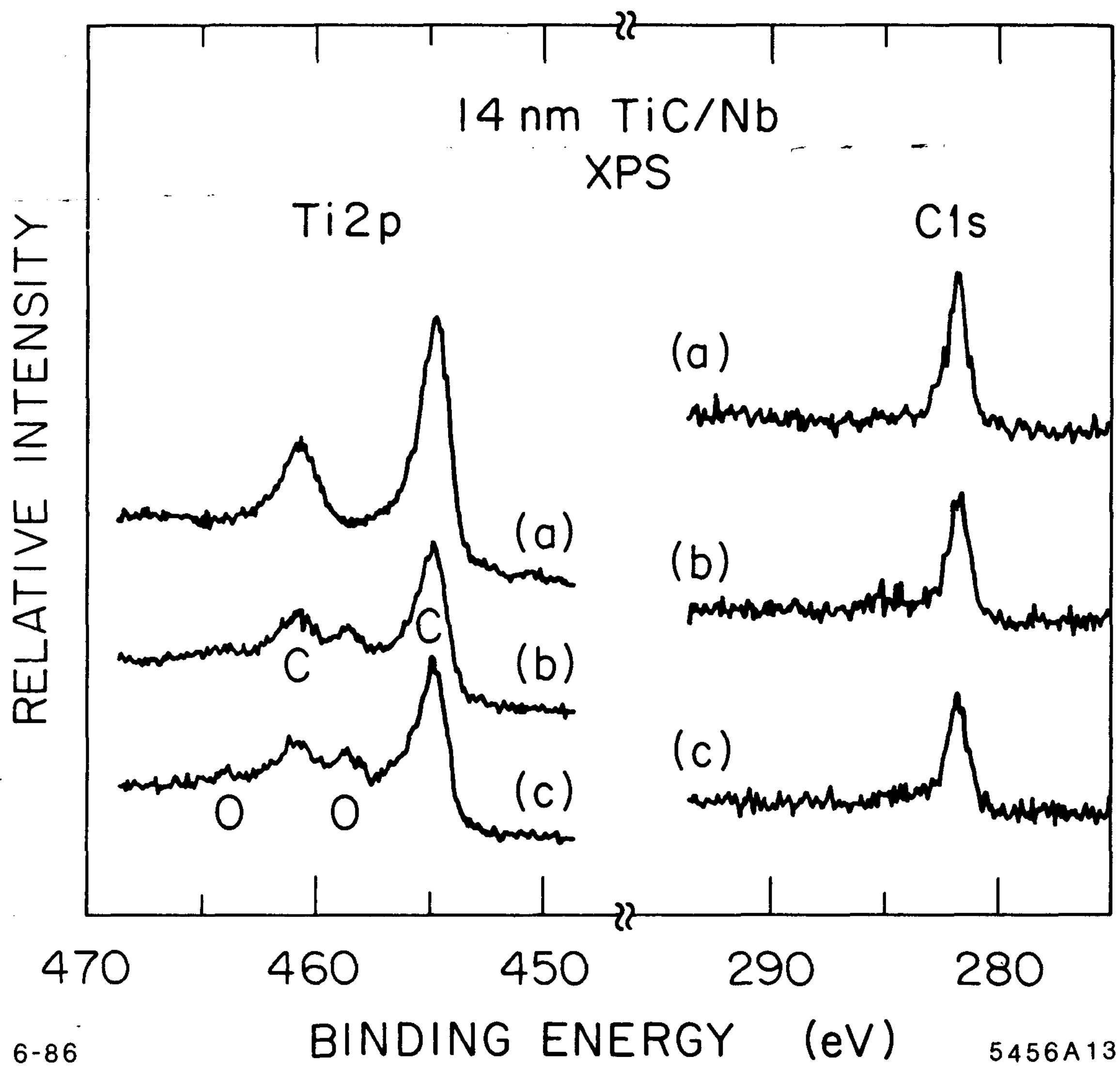

Fig. 13

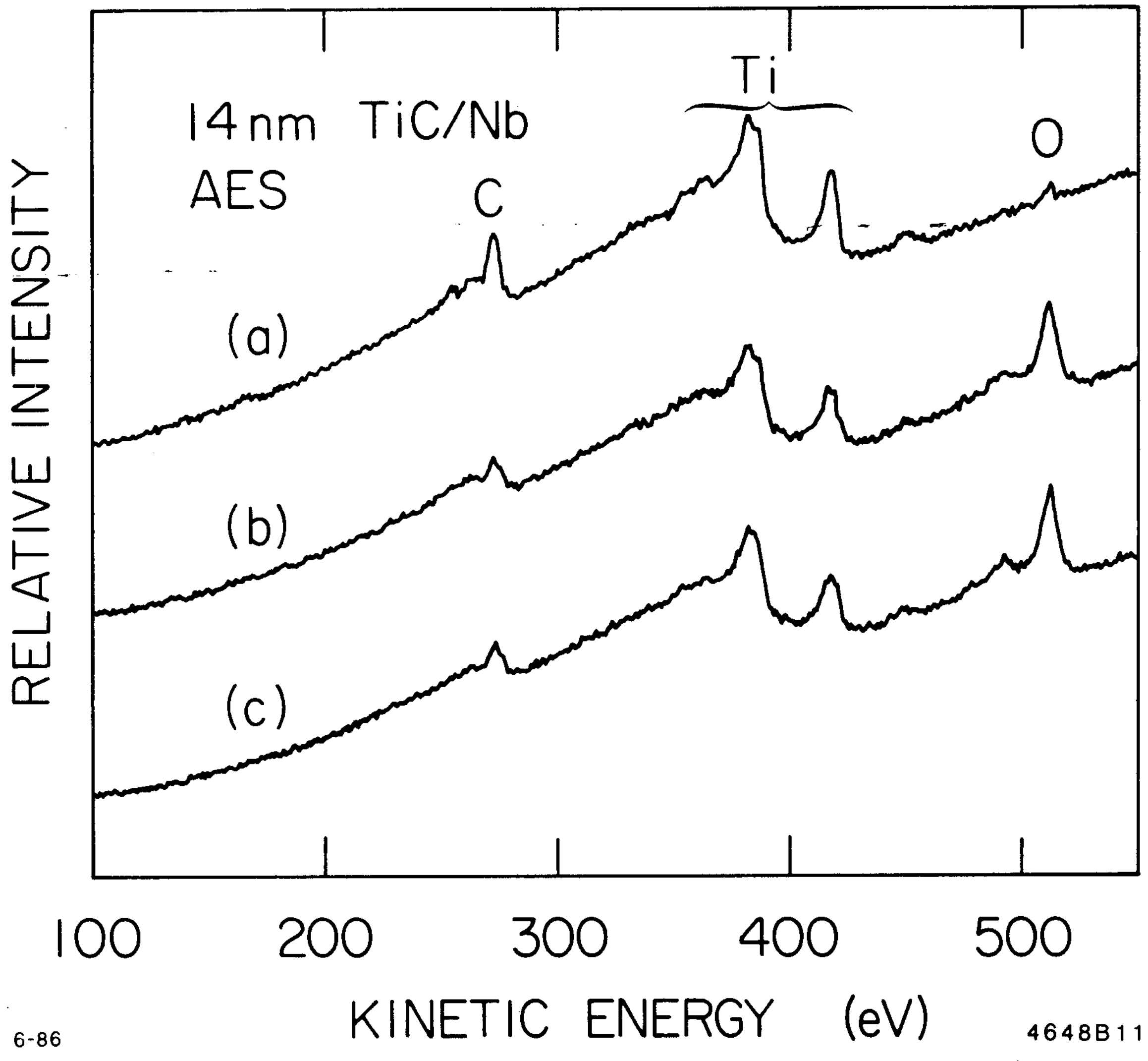

Fig. 14

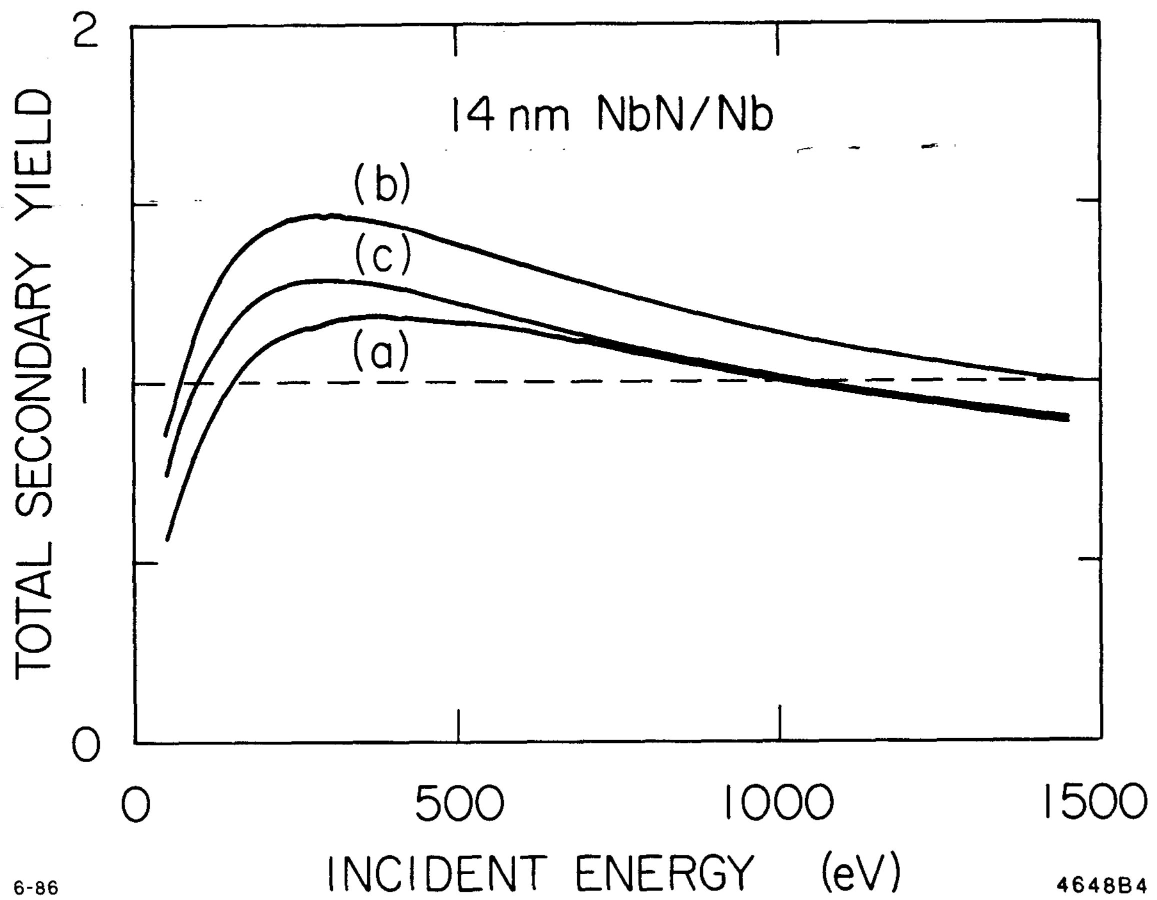

Fig. 15

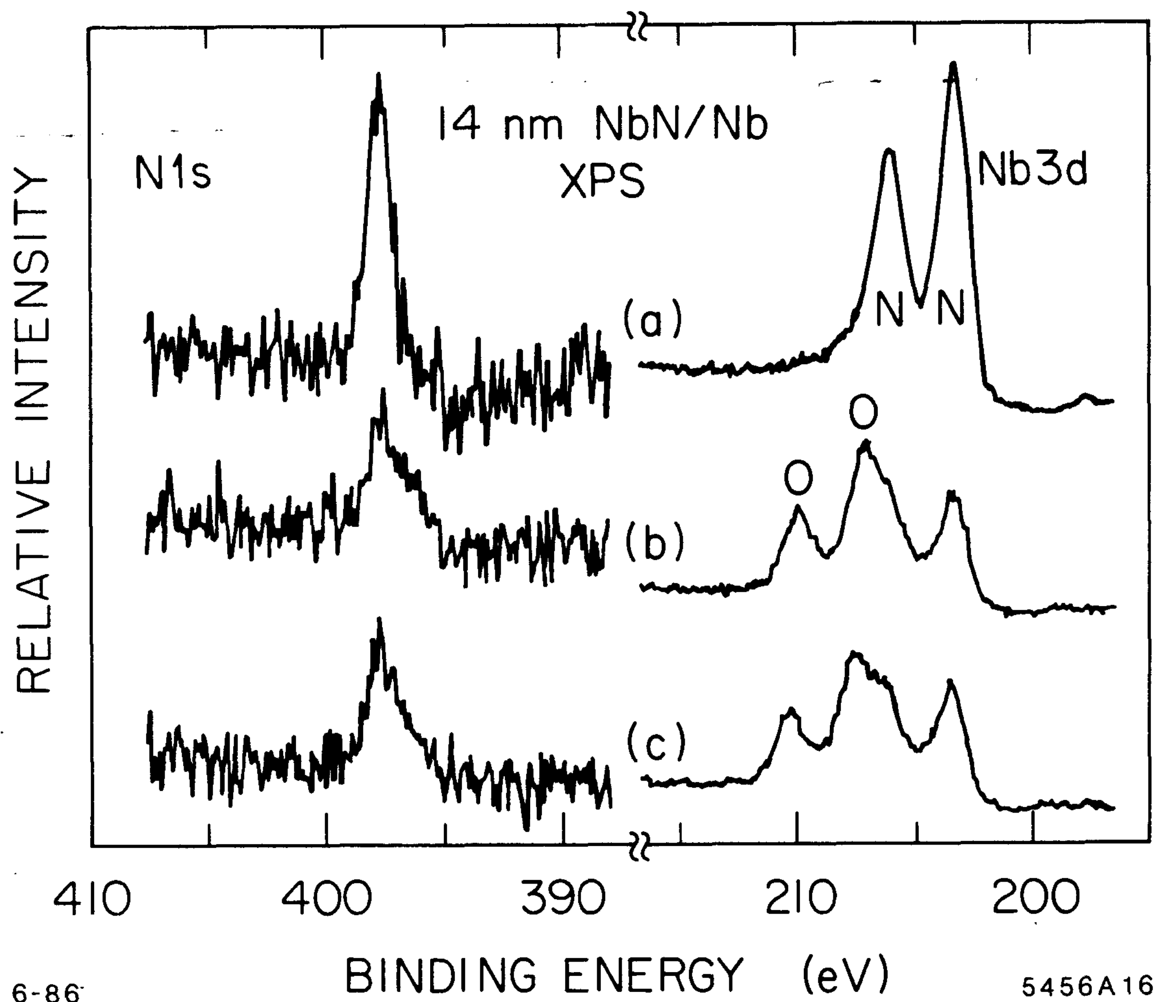

Fig. 16

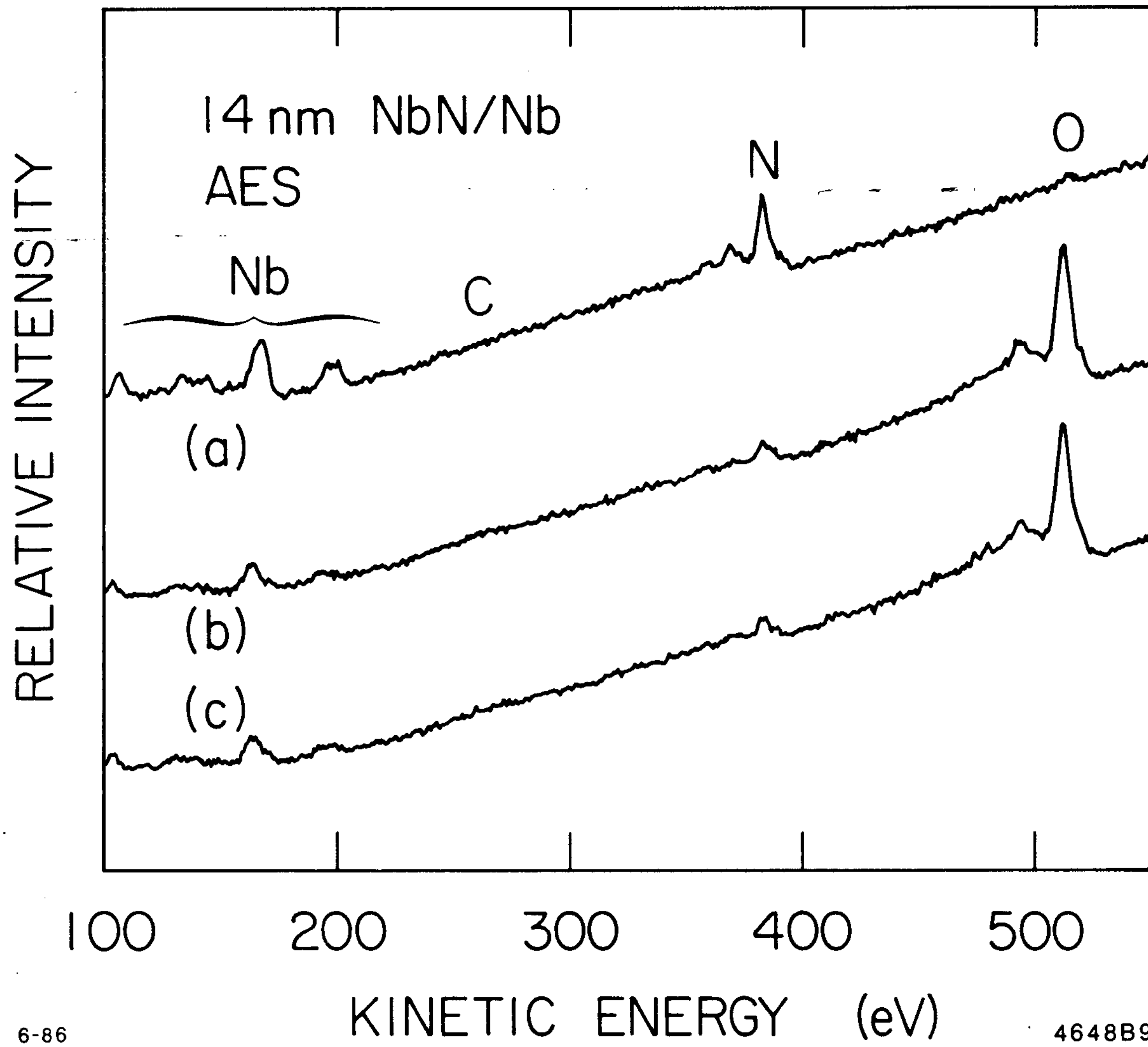

Fig. 17

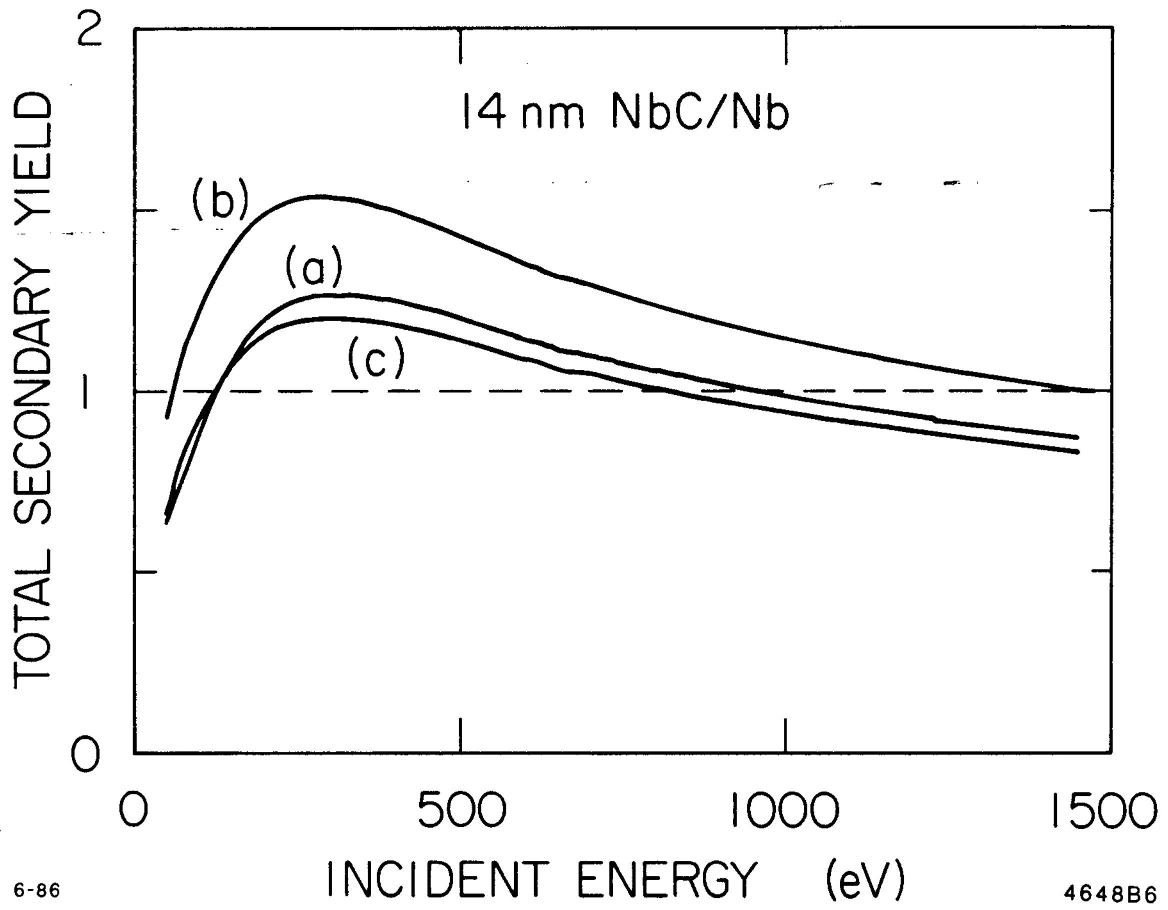

Fig. 18

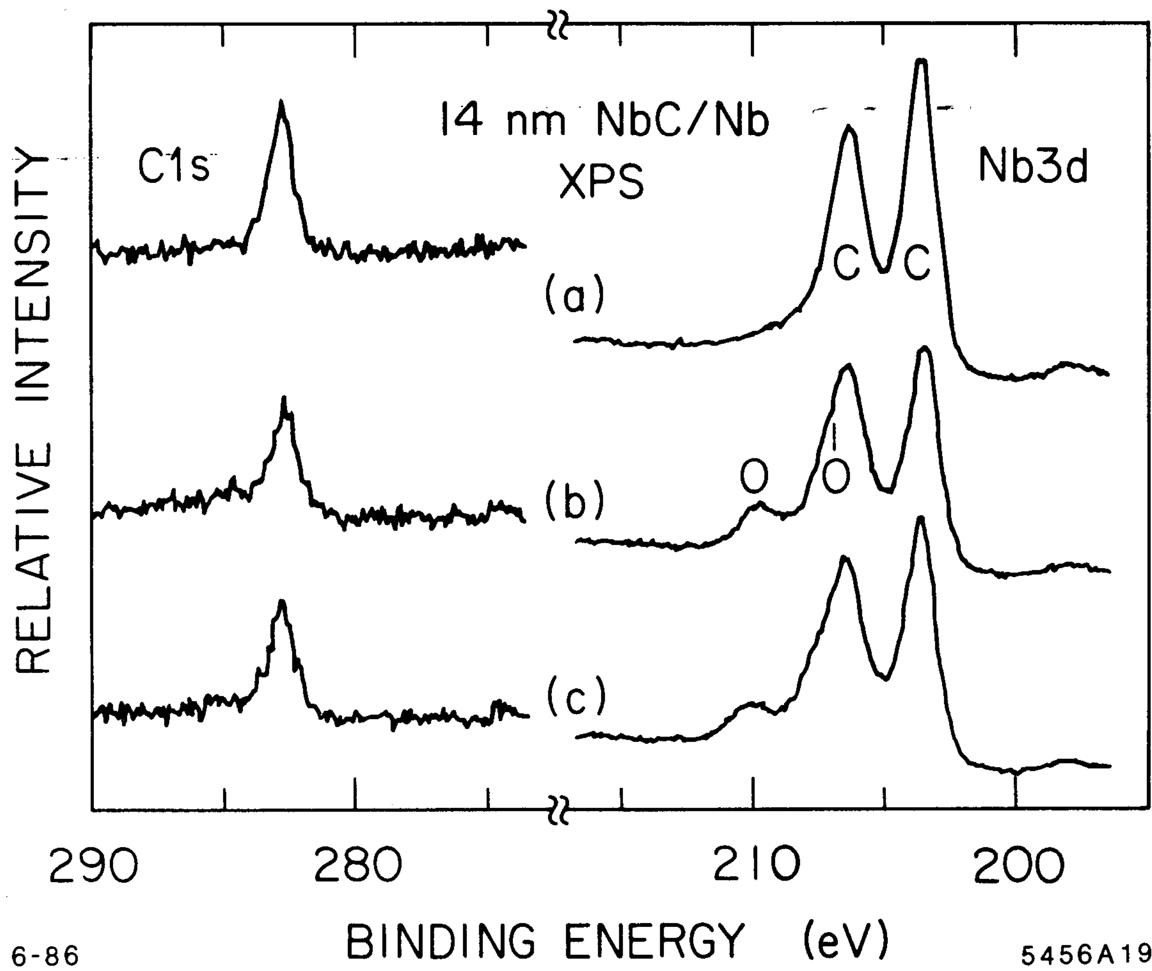

Fig. 19

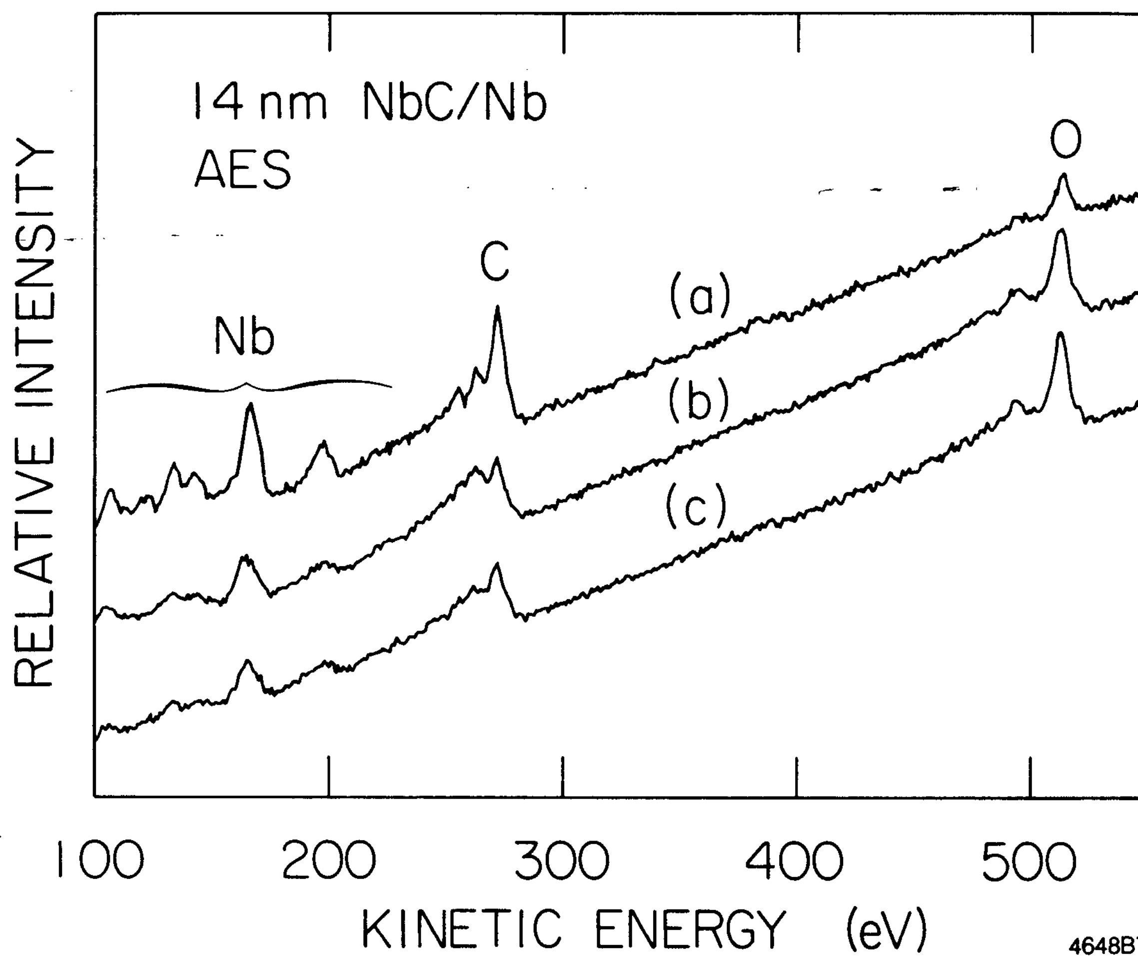

Fig. 20

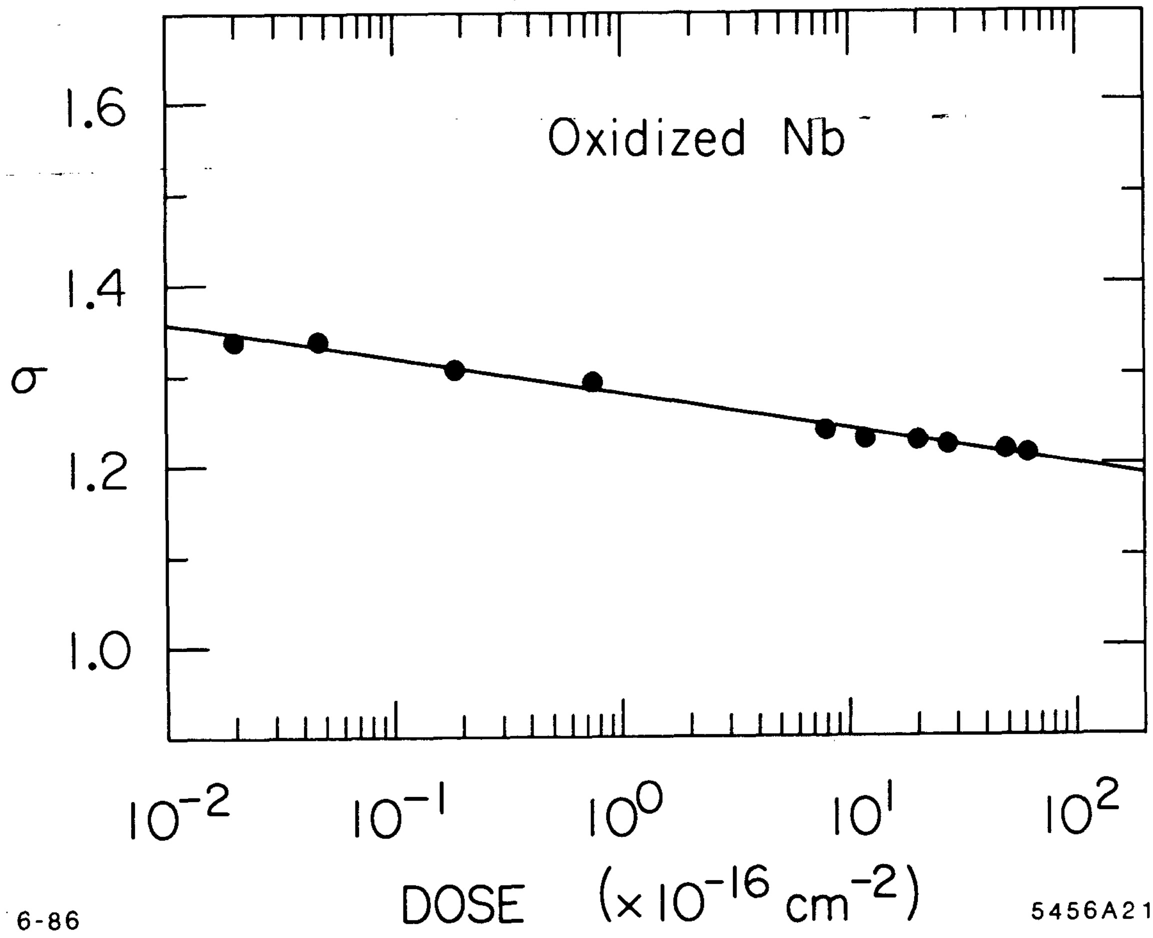

Fig. 21

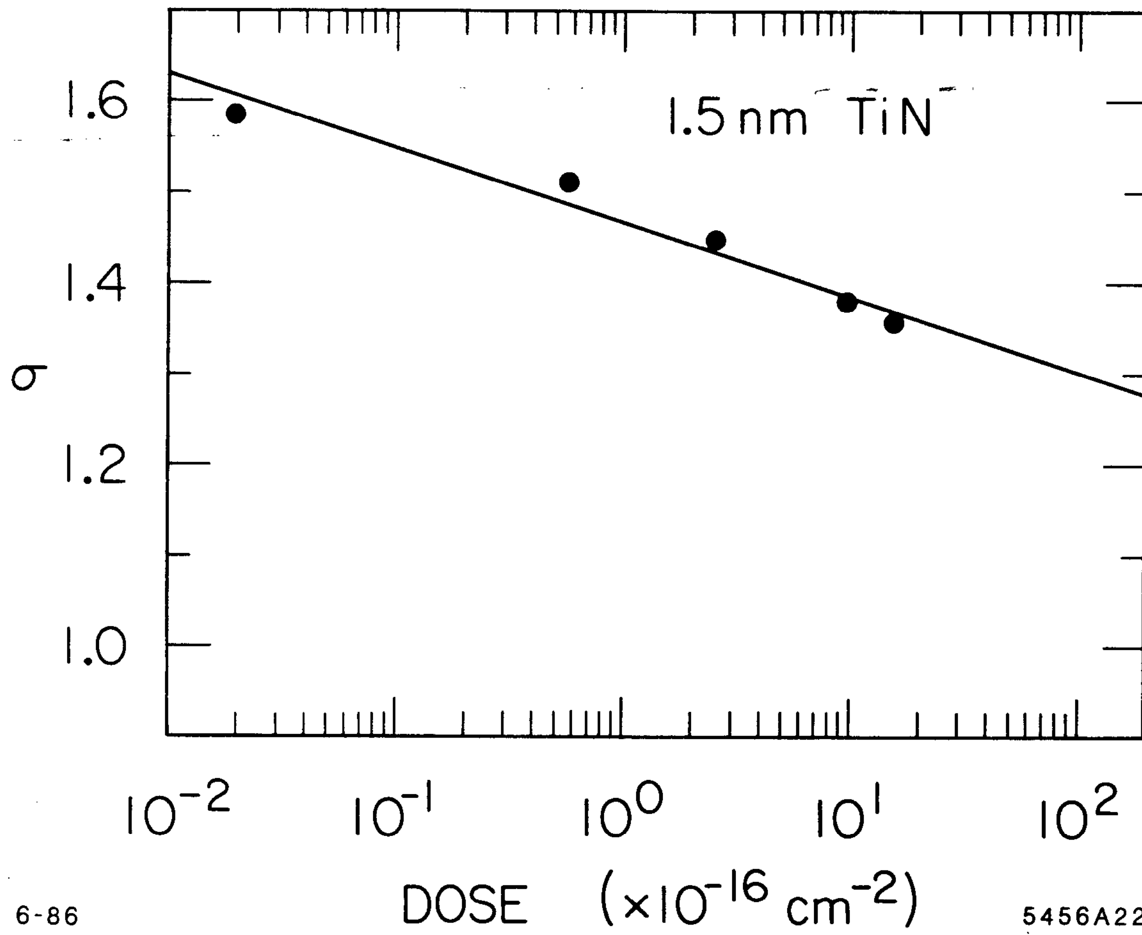

Fig. 22

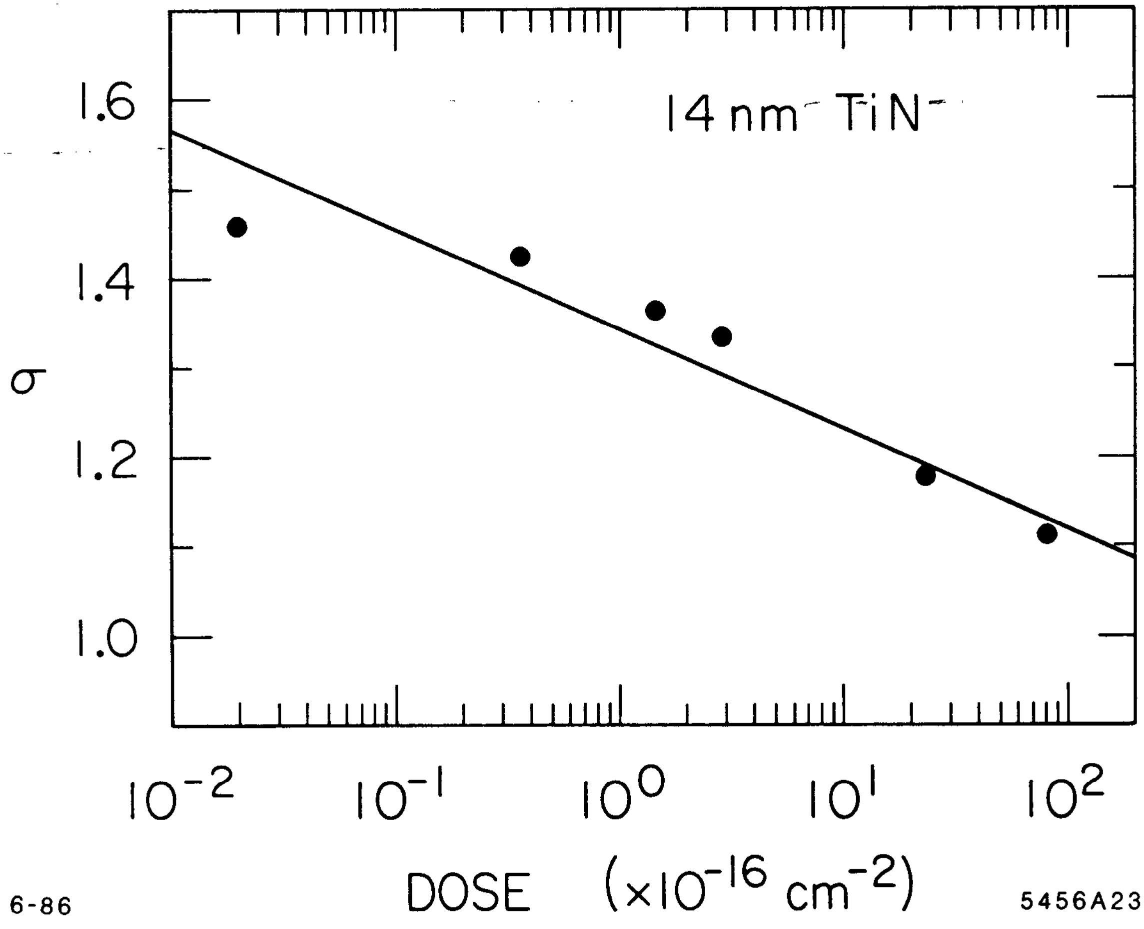

Fig. 23

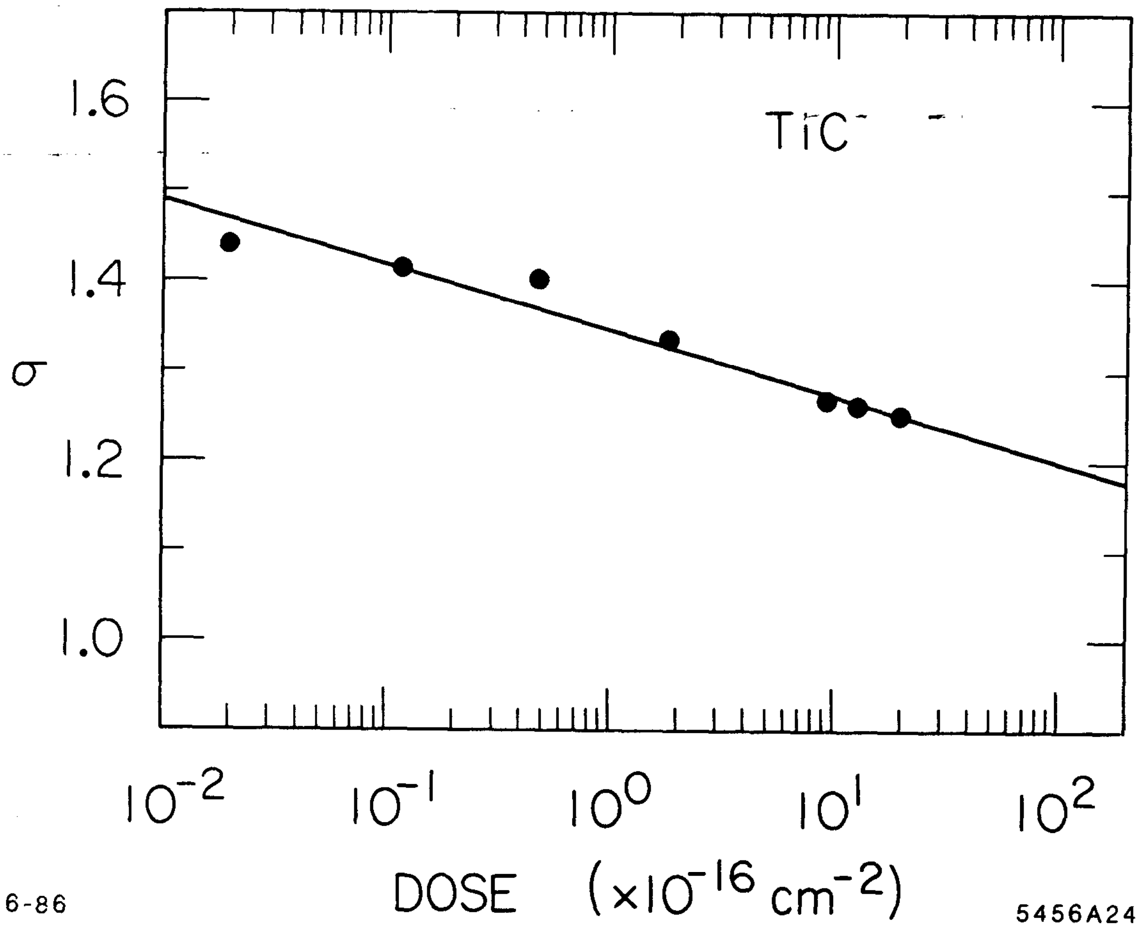

Fig. 24

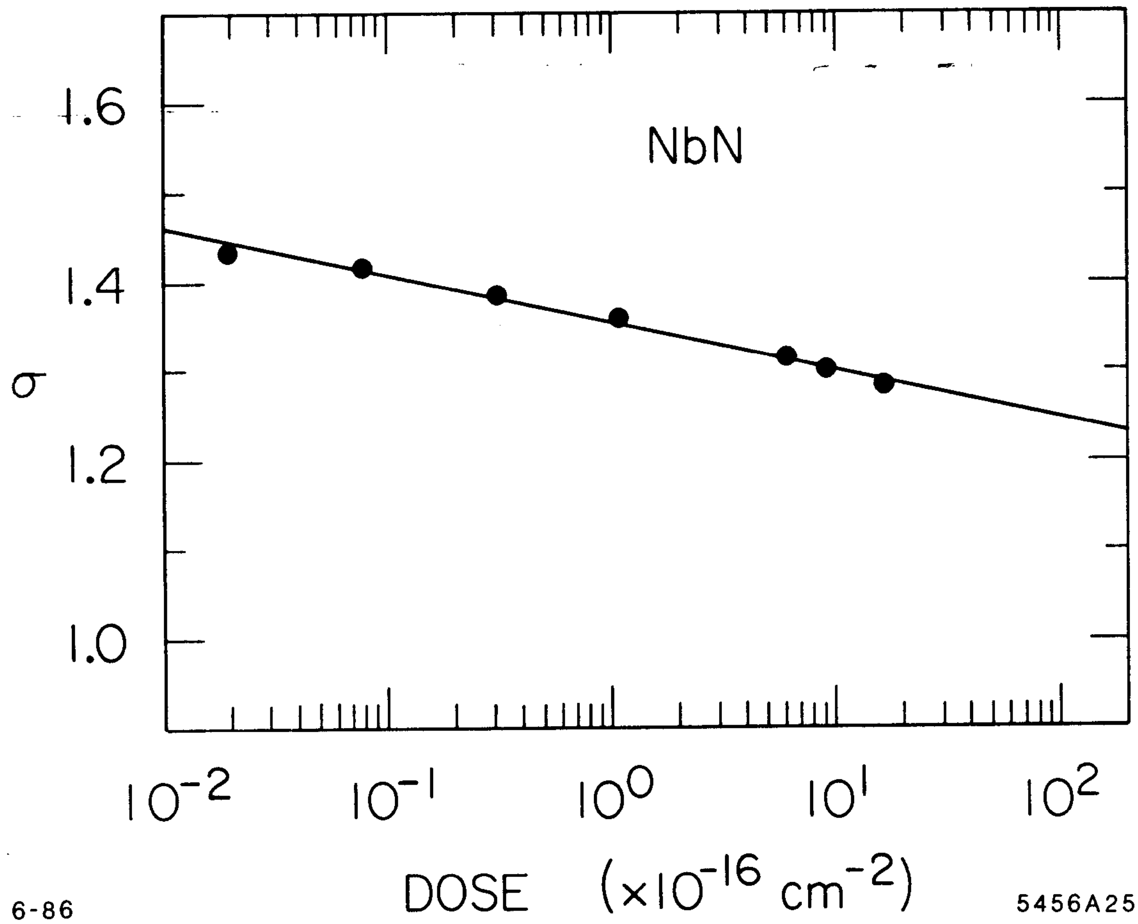

Fig. 25

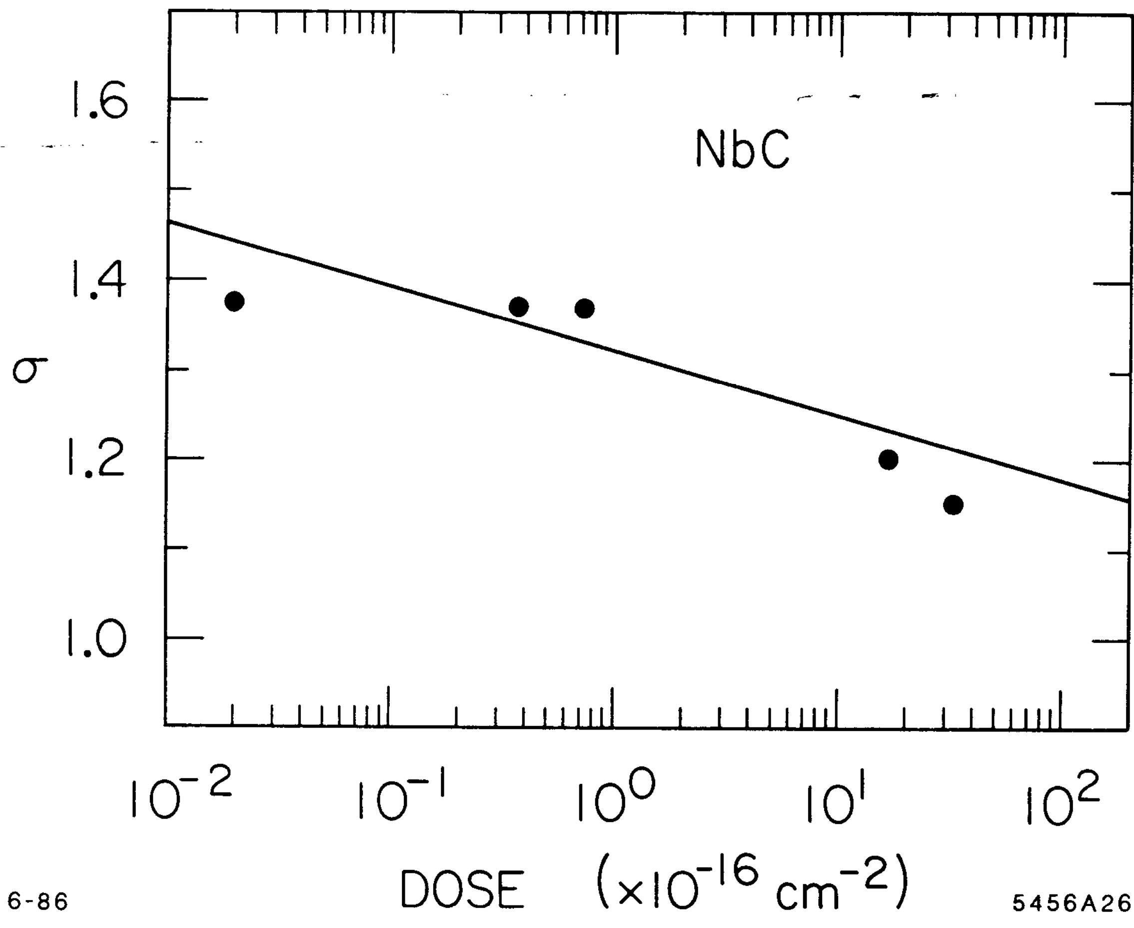

Fig. 26